Evaluations of Simulation Models for Flicker and Harmonics

Master's thesis in Sustainable Electric Power Engineering and Mobility

Petter Enlund & Arvid Erlandsson

DEPARTMENT OF ELECTRICAL ENGINEERING

CHALMERS UNIVERSITY OF TECHNOLOGY
Gothenburg, Sweden 2026
www.chalmers.se

Master's thesis 2026

Evaluations of Simulation Models for Flicker and Harmonics

Petter Enlund & Arvid Erlandsson

CHALMERS
UNIVERSITY OF TECHNOLOGY

Department of Electrical Engineering
Electric Power Engineering
Chalmers University of Technology
Gothenburg, Sweden 2026

Evaluations of Simulation Models for Flicker and Harmonics
Petter Enlund & Arvid Erlandsson

© Petter Enlund & Arvid Erlandsson, 2026.

Supervisor: Jon Rasmussen, Hitachi Energy
Examiner: Massimo Bongiorno, Division of Electric Power Engineering

Master's Thesis 2026
Department of Electrical Engineering
Division of Electric Power Engineering
Chalmers University of Technology
SE-412 96 Gothenburg
Telephone +46 31 772 1000

Typeset in LaTeX
Printed by Chalmers Reproservice
Gothenburg, Sweden 2026

Evaluations of Simulation Models for Flicker and Harmonics

Petter Enlund & Arvid Erlandsson
Department of Electrical Engineering
Chalmers University of Technology

Abstract

Electric arc furnaces (EAF) are highly dynamic industrial loads that exhibit rapid variations in active and reactive power draw. These dynamics introduce significant power quality disturbances at the point of common coupling (PCC). To mitigate this, a Static Synchronous Compensator (STATCOM) is connected in parallel to dampen the current variations and therefore the power quality disturbances. To size the STATCOM well, preliminary studies with accurate EAF and STATCOM models are vital.

This thesis evaluates if a publicly available STATCOM and EAF model can be reliably used to study power quality disturbances. This will be done by comparing the public models with Hitachi's detailed STATCOM and EAF model based on current measurements. The public EAF model uses a mathematical formula of an arc that emulates flicker behavior with random noise and a non-linear V-I relationship. The public STATCOM has a simple control scheme that works by averaging the current variations from the EAF model and subtracting the variations from the average current.

The results indicate that the mathematical EAF model can reproduce the flicker levels observed in the measurement-based model. However, the flicker originates from other frequencies and has a different flicker distribution, overemphasizing the commonly occurring flicker content. Furthermore, the harmonic spectrum of the mathematical EAF model is inaccurate, the second harmonic is 27.6% lower, while the third harmonic is 30.0% higher than in the current measurement model. The public STATCOM model also shows limited accuracy. It only reduced flicker by an average factor of 3.47 compared with the Hitachi's model that reduced it by an average factor of 7.53. In addition, the public STATCOM increases the current total demand distortion (TDD) by an average of 43.1% compared to a 6.5% decrease for the Hitachi model, and it lacks power factor (PF) control capability.

To improve the mathematical EAF model further the second harmonic and interharmonic-group would need to be increased and more apparent power peaks would need to introduced. The public STATCOM model could be improved by incorporating d-current flicker control, dedicated power factor control and a current rate limiter. In its current form the mathematical EAF model is not suitable for estimating flicker or harmonics. Moreover, due to its poor flicker and harmonic performance the STATCOM cannot be used. Therefore, STATCOM sizing studies are unsuitable to do with the public model.

Keywords: EAF, STATCOM, Power Quality, Flicker, Harmonic, Interharmonic, Negative Sequence, Power Factor.

Acknowledgements

First and foremost, we would like to thank our supervisor Jon Rasmussen at Hitachi Energy for his enthusiasm, technical expertise and support. Without your help and feedback the project would never be complete. We would also like to thank Massimo Bongiorno for being our examiner.

We would also like to thank out collages at Hitachi Energy for the numbers fun and interesting conversations. You guys really made us feel like a part of the team.

Finally we would like to thank our families for the support throughout all the years at Chalmers. I, Petter, would especially like to thank my brother Albert for all the positivity, strength and support you have given me during this thesis.

Petter Enlund & Arvid Erlandsson, Gothenburg, June 2026

List of Acronyms

Below is the list of acronyms that have been used throughout this thesis listed in alphabetical order:

DPF	DIgSILENT Power Factory
EAF	Electrical Arc Furnace
EMT	Electromagnetic Transients
FACTS	Flexible AC Transmission System
FFT	Fast Fourier Transform
HVDC	High Voltage Direct Current
PCC	Point of Common Coupling
PF	Power Factor
PLL	Phase Locked Loop
RMS	Root Mean Square
STATCOM	Static Synchronous Compensator
SVC	Static Var Compensator
TDD	Total Demand Distortion
THD	Total Harmonic Distortion
TSO	Transmission System Operator
VMACH	Virtual Modular Advanced Control System for HVDC
VSC	Voltage Source Converter

Contents

List of Figures

List of Tables

1
Introduction

1.1 Background

With an increasing converter based generation and load, present regulations for power quality face risks of being insufficient in upholding distribution quality standards. As such, standards might change to account for this growing problem which would force industries to comply in ensuring that they do not further pollute the grid. One source of pollution is the (EAF), industrial loads used to melt metal with the use of high current electrical arcs. These arcs are very hard to model because of changing load asymmetry, making it a continuous transient system since a steady state is never reached. For this reason, the active and reactive power also follow the same transients which work to pollute the power quality, resulting in phenomena such as voltage flickers and harmonic distortion. To mitigate these effects a STATCOM is commonly used to counteract variations seen by the grid. The STATCOM use power electronics to change its reactive power output to stabilize the voltage at the point of common coupling (PCC), and is better suited for flicker and harmonic mitigation as opposed to a thyristor based compensator as the switches can be turned off before the current zero crossing. Because of complexity and high investment costs, accurate simulation models are important in STATCOM sizing to ensure grid compliance and overall business operation.

As the EAF has continuous, fast and transient dynamics which dictate the harmonic and flicker content, full electromagnetic transient (EMT) simulations are required for accurate representation of the EAF-STATCOM interaction. RMS simulations are good for steady state studies and slow power flow dynamics, but misrepresent fast transient behavior by averaging the waveform. This ends up either misrepresenting the EAF characteristic or manipulating the EAF input data in such a way that performance results may be misleading.

Many approaches have been used to model EAFs. In [1] and [2] mathematical models using a random number generator to represent the dynamic behavior of an EAF were tried. Meanwhile other studies [3], [4] and [5] used recorded data from real EAFs in their models to capture all behaviors of EAFs. The EAF measurements were used to feed different source equivalents. Both current and voltage-impedance equivalents were used. Different simulation software was used for these studies. PSCAD is commonly used as it is built for EMT simulations.

In PSCAD, Hitachi has built a virtual emulation of their STATCOM controller called Modular Advanced Control System for HVDC (MACH or vMACH for the PSCAD controller), containing virtual representations of the control-cabinets and communication-schemes [6]. This allows for very accurate simulations of how an actual STATCOM controller functions and reacts to EAF dynamics. For STATCOM sizing Hitachi use the vMACH together with an EAF model based on a current source that inputs recorded EAF current data [6]. Another common tool used to simulate EAFs and STATCOMs is DIgSILENT PowerFactory (DPF) [6]. DPF is a software that can perform load flow calculations, RMS and EMT simulations among others. In DPF a prebuilt model of an EAF based on a stochastic mathematical model exists together with a simple STATCOM model with flicker control.

1.2 Aim

This thesis aims to evaluate whether publicly available models can be used to reliably study power quality effects related to EAFs and whether the results are applicable for STATCOM sizing. To achieve this the DPF model will be used and compared with the Hitachi model.

1.3 Research Questions

- How accurately does a mathematical EAF model represent the negative power quality effects induced by an EAF compared with a measurement based model?
- How accurately does a simplified publicly available STATCOM model compensate the negative power quality effects induced by an EAF compared with a detailed STATCOM model?
- Based on the questions above, to which extent can the public model be used for STATCOM sizing? How does the software affect these results?

1.4 Limitations

- Only AC EAFs will be simulated.
- This report only evaluates power quality effects related to flicker, harmonics, interharmonics, negative and zero-sequence.
- The EAF measurement model will be used as reference when evaluating models. This is done as Hitachi uses this model to size their STATCOMs.
- The vMACH will be used as reference for STATCOM models. This is done as it is a very accurate representation of a real STATCOM that is used in industrial applications.
- Because the vMACH is Hitachi's intellectual property it cannot be explained in detail.
- The project does not aim to study any STATCOM control or parameter optimization in detail.

2

Theory

2.1 EAF Types and Operation

There are many types of EAFs, and they are primarily categorized in AC and DC furnaces. Figure 2.1 shows a very simple schematic of the three phase AC furnace.

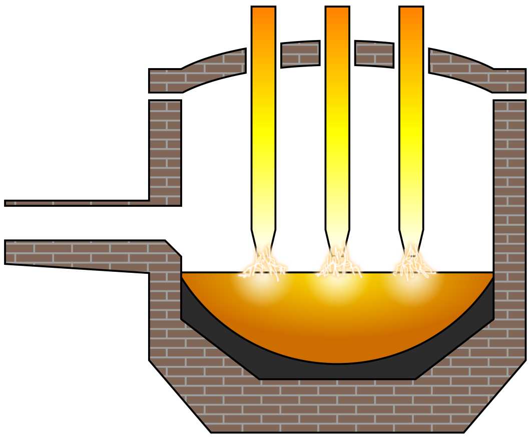

Figure 2.1: Simple AC EAF design for bucket charging from [7].

The furnace is fed electricity from three movable electrodes that control the strength of the arc depending on the altitude and exposure to the scrap material [8]. Before operation, the top valve is swung to the side for charging of the furnace, the process by which raw scrap material is added for melting [8]. Afterwards the lid is closed and the electrodes are lowered to start the melting [8]. The design in Figure 2.1 can be tipped to pour the melt, but industry applications usually have different methods as the designs can grow very large [8]. Due to massive current draw and to protect the furnace shell from radiation both the EAF and cables feeding the electrodes are water cooled [8].

Figure 2.2 shows a general grid connection for industry application EAF:s. The industrial connection is made immediately at the 132 kV distribution level which is connected through a high voltage (HV) 132/33 kV transformer to a 33 kV bus, called the dirty bus as it needs to be isolated from other industry appliances and local loads due to the EAF power quality pollution [8]. The transformer is often configured to DNy to remove zero-sequence current, but other configurations exist where both sides are directly grounded [6].

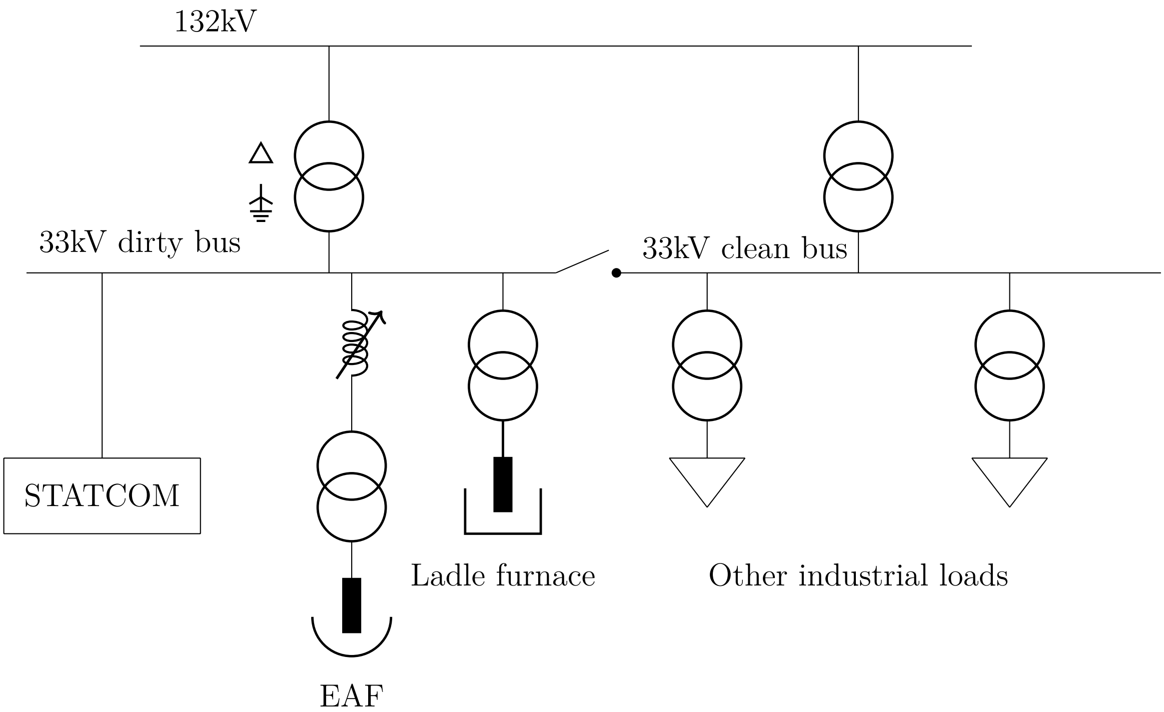

Figure 2.2: Industrial EAF and STATCOM grid connection

Other furnace equipment and compensating devices are also located on this bus, for example the ladle furnace, shown in Figure 2.2, which is a smaller EAF often used to refine and finalize the bath. This involves temperature and chemical composition control and has a gentler operation than the EAF [8]. The furnace connection consists of an EAF transformer and often a variable reactor for reactive power control. Both the HV and EAF transformers are equipped with tap changers for voltage control [9]. To meet transmission system operators (TSO) grid codes for voltage flicker and other power quality effects produced by the EAF compensating devices are installed in shunt, usually STATCOMs for their ability to react to rapid changes at the dirty bus.

The AC EAF is the most common furnace and can be operated using bucket charging and continuous charging [8]. Bucket charging involves discretizing the operation in phases of charging and melting whereas continuous charging uses a conveyor belt style layout, always feeding the furnace during operation [8]. This is typically called the consteel process. A typical bucket charge operation is shown in Figure 2.3 [10]. Note that the profile shown is arbitrary and serves to communicate a general characteristic attributed to the bucket EAF. Profiles vary between producers and models.

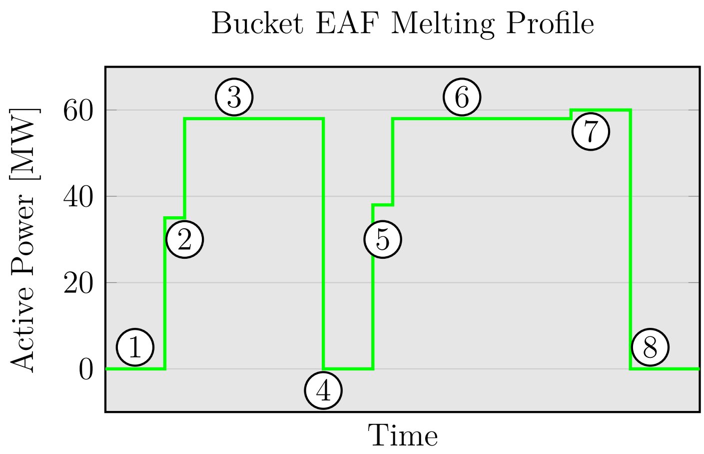

Phase	Description
1	Preparation and charge
2	Boring phase
3	Melting
4	Charge
5	Boring phase
6	Melting
7	Superheating (refining)
8	Tapping

Figure 2.3: Bucket charge EAF melting power profile with phase definition and furnace load state.

The process can generally be sorted into charging, boring, melting, superheating and tapping [11], [8]. The distinction is made as every work cycle often requires the scrap to be melted from the beginning with different stages in the process requiring different working conditions. The furnace is controlled with the series reactor and tap changer to control the voltage and consequently the power factor (PF) of the EAF [9]. The PF operating point is between 0.7-0.9 and is shown in Figure 2.4 with different operating points for an EAF maintaining 300 MVA [6].

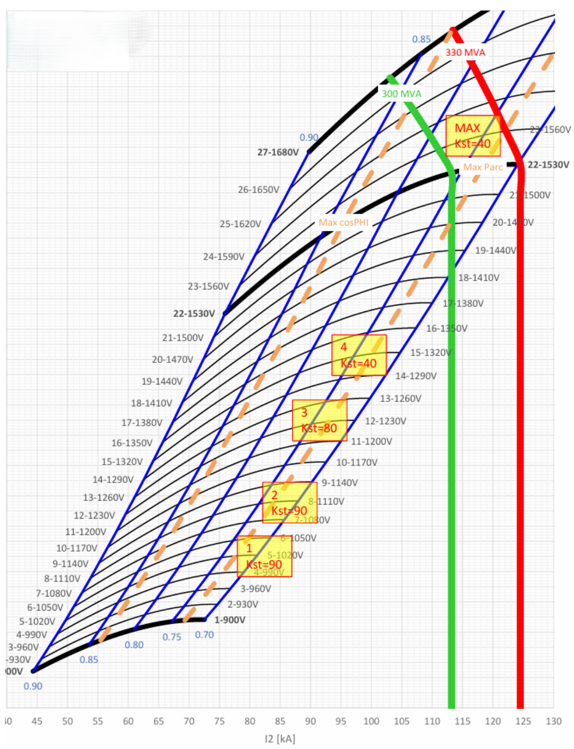

Figure 2.4: EAF operating point diagram

The work cycle begins with charging of the EAF, where the furnace lid is moved to unload the scrap bucket [8]. It is common for the furnace to contain leftover melt from the previous operation, or for portions of the scrap material to be otherwise preheated to accelerate the process [11], [8]. This is often the case when using a double-furnace design where the electrode arm can be moved between the two buckets, increasing operation up-time. Here the preheating is done by transporting hot fumes from one furnace to the other between operations [8]. A similar strategy is used in continuous charging, where the fumes are transferred from the operational furnace along the conveyor belt to preheat the scrap [8]. For the DC furnace pre-heating is required [11]. When the lid is closed the boring phase begins. This is the most demanding part of the operation, with rapidly varying power draw and asymmetry. Here, a lower PF is required to keep the arc ignited [11]. After a while the active power draw reaches its max as the operation enters the melting phase and lastly superheating phase when the scrap material is sufficiently melted [11], [6]. The PF is increased as the arc can be sustained and the substance is refined and heated to reach the desired temperature [11]. Afterwards the furnace is tipped and the melt is let out, known as tapping [11]. The work cycle takes around one hour with interruptions mid-session, typically one or two, for re-charging as the melted scrap material frees up space for additional material [8]. This is also shown in Figure 2.3.

Continuous charging instead has a longer operating phase where raw material is continuously added [8]. The benefit of the continuous charging EAF is that the melted material keeps a more even temperature throughout the operation, in turn managing a more even impedance profile that leads to less voltage fluctuations [8]. A single melting session can be performed over an entire week, thus lessening the impact on the grid [8].

The industrial DC EAF was introduced in the late 80's[8]. The principal operation and grid connection is the same as for the AC EAF, though the design uses a single movable electrode fed through a three phase rectifier connecting the arc to an electrode placed at the base of the furnace [8]. However, the controller in the rectifier changes the current draw based on current grid conditions more than an AC EAF. In Figure 2.5 a schematic of a DC EAF is displayed [8]. Dual electrode designs without bottom electrode also exist [8]. In Figure 2.6 the principal diagram of a twelve pulse fed DC-EAF is displayed.

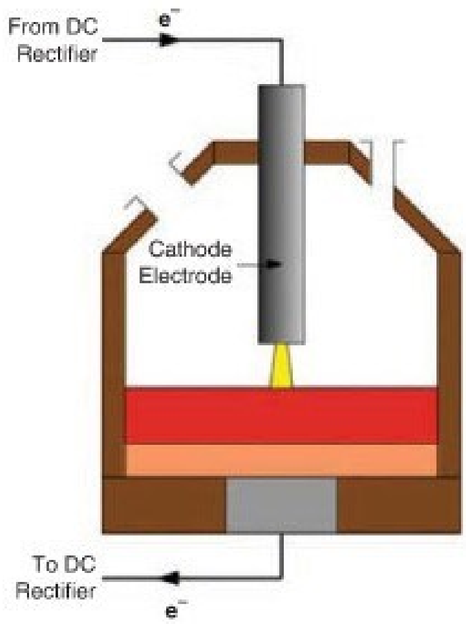

Figure 2.5: Simple DC EAF adapted from Fig. 1 in [12]

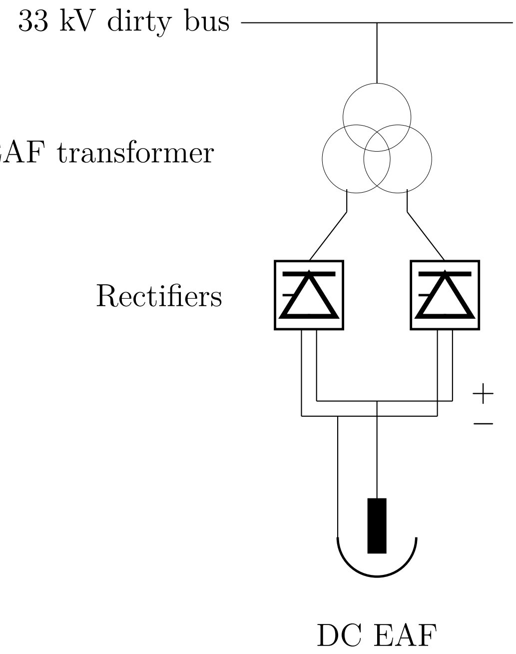

Figure 2.6: 12-pulse DC EAF principal operation

The DC furnace offers better performance with regards to voltage flicker and noise during operation [11]. Drawbacks are investment and operational costs from the rectifiers and continuous maintenance of the bottom electrode [11].

Both AC and DC EAF will experience movements in the mechanical structure due to the large electromagnetic forces [13]. These movements are called secondary system oscillation and usually have an oscillating frequency between 2-5 Hz [13]. The mechanical oscillation will move the electrodes witch in turn will change the arc length and therefor introduce the same oscillation in the phase current [13].

2.1.1 Different EAF Modeling Approaches

EAFs have been modeled in different ways. In [1] the authors modeled the EAF like a random resistance $R(t)$ according to (2.1) where ω_L and ω_H are random frequencies with concentration around 8 and 30 Hz respectively. a_L and a_H are randomly generated magnitudes ranging from 0 to 50 and 0 to 10 respectively [1]. ω_L, ω_H,a_L and a_H values are updated every zero crossing and the phase angels θ_L and θ_H are calculated to ensure continues waveforms [1]. R_0 is a constant resistance, t is time. [1].

$$R(t) = R_0 + a_L \cos(\omega_L t + \theta_L) + a_H \cos(\omega_H t + \theta_H)[\Omega] \tag{2.1}$$

In [2] the authors used a mathematical function combining both a hyperbolic (2.2) and an exponential (2.3) equation to make the best possible representation where the hyperbolic function was used to represent the low order currents and the high order by the exponential part (2.4) [2]. $v_{hyp}(i)$, $v_{com}(i)$ and $v_{exp}(i)$ all denotes the arc voltage, i the arc current, C is the arc power, while D is the arc current constant [2]. V_{at} denotes the voltage threshold that the arc voltage approaches as the arc current increases. I_0 is the maximum current [2]. The function $O(i)$ (2.5) is a transition function that depends on the arc current i and controls the weighting between the two models [2]. The parameter I_t denotes the transition current that defines the current level at which the model transitions between the exponential and hyperbolic behaviors [2].

$$v_{hyp}(i) = V_{at} + \left(\frac{C}{D+i}\right) \tag{2.2}$$

$$v_{exp}(i) = V_{at}(1 - e^{i/I_0}) \tag{2.3}$$

$$v_{com}(i) = [1 - O(i)] \cdot v_{exp} + O(i) \cdot v_{hyp} \tag{2.4}$$

$$O(i) = e^{\left(\frac{-i^2}{I_t^2}\right)} \tag{2.5}$$

In [3] the authors used real voltage and current data from an EAF, rescaled to values a converter could manage to build a power-electronic-based emulation (PEBE). The converter that emulated the EAF in the lab was controlled by a generalized predictive power control (GPPC) to emulate the waveforms seen in the data and therefor no mathematical model of the EAF was needed [3].

In [4] the authors described two classical ways of modeling an EAF when measured data is available. The first one is called harmonic current injection model (HCIM) and it works by injecting the measured current from the EAF into the EAFs secondary side of the transformer [4]. The second one is called harmonic voltage source model (HVSM) it works by modeling the EAF as a voltage source behind the secondary side impedance [4]. The measured voltage is at the secondary of the EAF transformer. The calculation and circuit is displayed in equations (2.6),(2.7) and Figure 2.7 [4].

$$V_{cable}(t) = I_{arc}(t) \times Z_{cable} \tag{2.6}$$

$$V_{arc}(t) = V_{measured}(t) - V_{cable}(t) \tag{2.7}$$

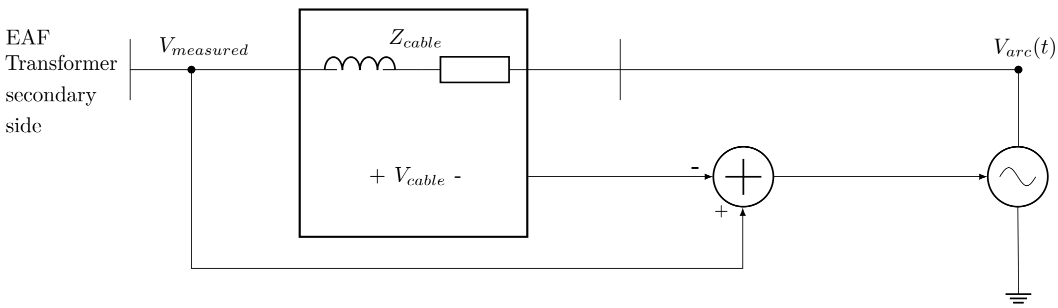

Figure 2.7: Arc voltage impedance model

2.1.2 PowerFactory Random Noise Model

In DPF there exists a prebuilt project featuring an AC EAF compensated by a STATCOM. Figure 2.8 shows the grid equivalent and Table 2.1 the system parameters.

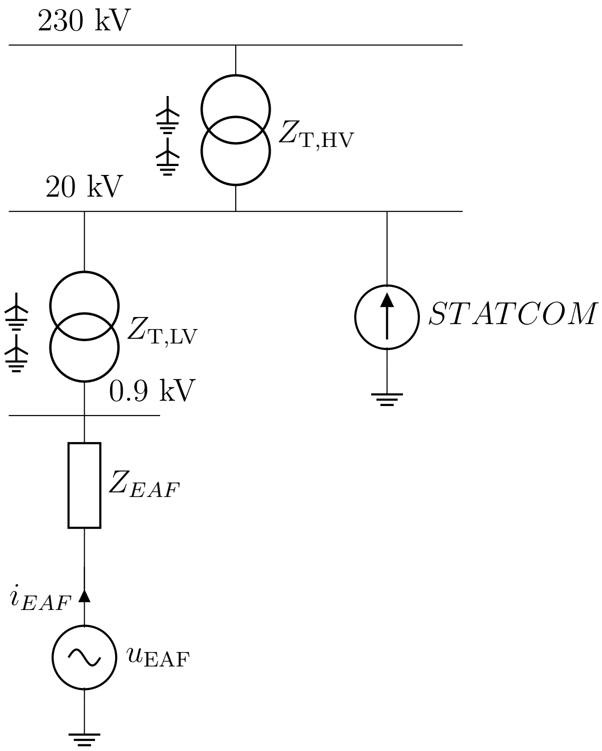

Figure 2.8: DPF original grid connection with random noise model EAF and STATCOM.

Parameter	**Value**	**Unit**
Grid		
S_{grid}	1300	[MVA]
X/R	25.12	
T_{HV}	230/20	[kV]
$S_{\text{T,HV}}$	200	[MVA]
$L_{\text{T,HV}}$	0.14	[pu]
$R_{\text{T,HV}}$	0.005	[pu]
T_{LV}	21/0.9	[kV]
$S_{\text{T,LV}}$	120	[MVA]
$L_{\text{T,LV}}$	0.0796	[pu]
$R_{\text{T,LV}}$	0.0025	[pu]
EAF		
S_{EAF}	137	[MVA]
L_{EAF}	9.550	[μH]
R_{EAF}	0.300	[mΩ]
STATCOM		
I_{rated}	968.74	[A]

Table 2.1: Original Random noise model parameters.

The grid is by default supplied by 2 synchronous generators and has some other load connections. The STATCOM is implemented as a current source with an implemented control model that is given in detail in section 2.3.3. The current source is grounded by default. Both transformers are directly grounded and use YNyn configurations. The EAF is implemented as a voltage source u_{EAF} behind an impedance Z_{EAF}. This is also grounded by default.

The furnace model is based on [14] which uses a piecewise-linear V-I characteristic that models the voltage based on the time variation of the arc-length based on a random noise input. Beginning with the single phase arc voltage

$$u_{EAF} = u_{EAF}(i_{EAF}) \tag{2.8}$$

it is described as having a non-linear current-relationship by

$$u_{EAF} = u_{EAF,t} + \frac{C}{D + i_{EAF}} \tag{2.9}$$

where C and D are constants used to relate the slope of the current to the increasing and decreasing parts of the V-I characteristic and $u_{EAF,t}$ is the base threshold value the voltage reaches when switching polarity [14]. It is calculated as

$$u_{EAF,t} = A + B \cdot l$$

where l is the arc length in cm and A is a constant accounting for the voltage drops across the anode and cathode [14]. B is the voltage drop per unit arc length [14].

Without any noise this model is in steady state, so to attribute the model with typical EAF characteristics such as flicker and voltage fluctuations it needs to be time-varying [14]. By changing (2.8) to

$$u_{EAF} = k \cdot u_{EAF,0}(i_{EAF}) \tag{2.10}$$

where k is used to determine the actual arc voltage V_a with arc length l from the base arc voltage $u_{EAF,0}$ corresponding to l_0, which is the maximum arc length suitable for continuous conduction[14]. By rearranging (2.10) k can be found

$$k = \frac{A + B \cdot l}{A + B \cdot l_0} \tag{2.11}$$

For varying l, white noise is introduced with reference to the base model as

$$l(t) = l_0 - r(t) \tag{2.12}$$

which, together with (2.11) give the time varying relationship of (2.13) [14].

$$k(t) = \frac{A + B \cdot l(t)}{A + B \cdot l0} = 1 - \frac{B \cdot r(t)}{A + B \cdot l_0} \tag{2.13}$$

The white noise is generated based on a number, called a seed, given to a random number generator. The DPF implementation of the random noise model calculates the phase voltages as per equations (2.9) and (2.13) with the phase currents as input. The calculation block diagram in Figure 2.9 illustrates this and the parameter values are found in Table 2.2 [14].

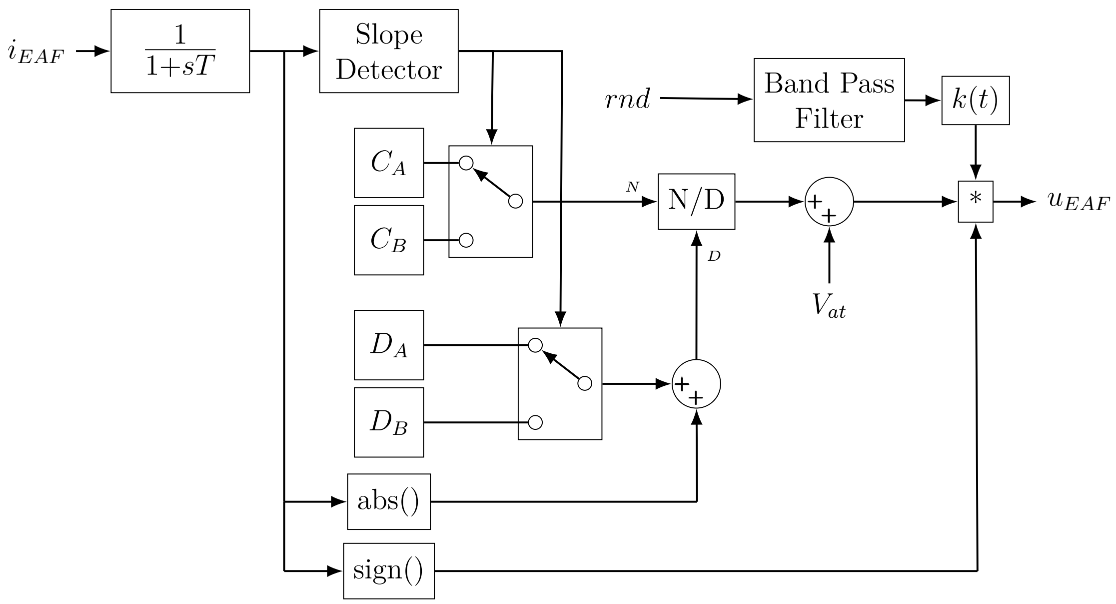

Figure 2.9: Single line voltage calculation block diagram.

The currents are first put through a lag filter and then fed to three different blocks, one of these being a slope detector that compares the last two values of i_{EAF} to determine the slope of the current as described in equation (2.14).

Parameter	Value	Unit
C_A	190000	[W]
C_B	39000	[W]
D_A	5000	[A]
D_B	5000	[A]
V_{at}	200	[V]
A	[40]	[V]
B	10	[V/cm]
l_0	10	[cm]

Table 2.2: Random noise model parameters

$$f(t) = \begin{cases} 1, & i^t_{EAF} > i^{t-1}_{EAF} \quad \wedge \quad |i^t_{EAF} - i^{t-1}_{EAF}| > 0.0001 \\ 0, & i^t_{EAF} < i^{t-1}_{EAF} \quad \wedge \quad |i^t_{EAF} - i^{t-1}_{EAF}| > 0.0001 \end{cases} \tag{2.14}$$

It outputs 1 for a positive slope on the condition that the absolute value of the slope exceeds 0.0001. The condition works as a dead-band. Conversely it outputs 0 on the negative slope given the same condition, otherwise the last output is kept. The logical values control the switch states C and D that outputs the different V-I relation values C_A, C_B, D_A or D_B.

At the last step the random noise is injected to the voltage. The noise works by generating a uniformly distributed value *rnd* between -1 and 1 with a frequency of 100 Hz. In DPF there are three methods for generating random noise. The Mersenne Twister, Linear Congruential and Additive Lagged Fibonacci method. By default, the Mersenne Twister method is used. The signal *rnd* is then passed through a second order band pass filter on the form shown in equations (2.15)-(2.17)

$$H(s) = \frac{H0 \cdot w_0}{Q} \frac{s}{w_0^2 + \frac{w_0}{Q}s + s^2} \tag{2.15}$$

$$w_0 = 2\pi\sqrt{f_{low} \cdot f_{high}} \tag{2.16}$$

$$Q = \frac{\sqrt{f_{high} \cdot f_{low}}}{f_{high} - f_{low}} \tag{2.17}$$

with parameters H_0=10, f_{high}=4Hz, f_{high}=14Hz. The filtered noise is then passed through equation (2.13) which is at last used to scale the output voltage u_{EAF}. The entire process is performed for each phase with different random noise seeds. This makes the model inherently unbalanced.

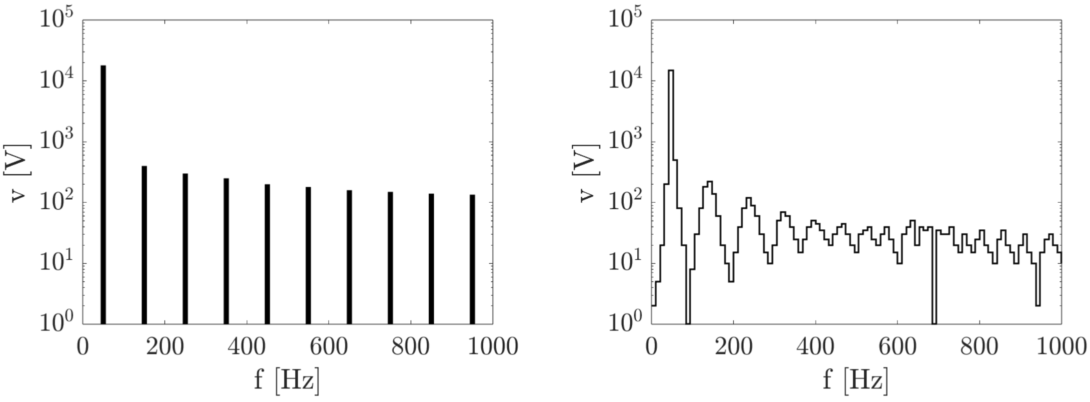

(a) Constant arc length

(b) Varying arc length

Figure 2.10: Harmonic analysis of the voltage at the dirty bus

The model resulted in the harmonic distribution shown in Figure 2.10. Only the odd harmonics originates from the arc model and the even come from the variations with the random arc length modulation [14].

2.2 Power Quality

2.2.1 Flicker

Flicker is the variation in the voltage magnitude below 50 Hz. An instant flicker value P_{inst} is defined in the standard IEC61000-4-15 and has a value one when 50% of the population notices the flicker in a 20 watt lamp [15]. The value of short term flicker severity P_{st} is equal to one when 50 % of the population would be irritated by flicker in the lamp and is calculated for a 10 minute period of weighted P_{inst} according to equation (2.18) [15]. The percentiles $P_{0,1}$, P_1, P_3, P_{10} and P_{50} are the flicker levels exceeded for 0,1; 1; 3; 10 and 50% of the time during the observation period [15]. The suffix “s” in the formula indicates that smoothed values should be used and are calculated according to equations (2.19)-(2.22) [15]

$$P_{\text{st}} = \sqrt{0.0314\,P_{0.1} + 0.0525\,P_{1s} + 0.0657\,P_{3s} + 0.28\,P_{10s} + 0.08\,P_{50s}} \tag{2.18}$$

$$P_{50s} = \frac{P_{30} + P_{50} + P_{80}}{3} \tag{2.19}$$

$$P_{10s} = \frac{P_6 + P_8 + P_{10} + P_{13} + P_{17}}{5} \tag{2.20}$$

$$P_{3s} = \frac{P_{2.2} + P_3 + P_4}{3} \tag{2.21}$$

$$P_{1s} = \frac{P_{0.7} + P_1 + P_{1.5}}{3} \tag{2.22}$$

Long term flicker severity P_{lt} is a cubic summation of the P_{st} values, calculated according to equation (2.23). For example, an $N = 12$ reflects a 2 hour P_{lt} value given 12 P_{st} values based on 10 minute intervals [15].

$$P_{\mathrm{lt}} = \sqrt[3]{\frac{\sum_{i=1}^{N} P_{\mathrm{st}i}^{3}}{N}} \tag{2.23}$$

To calculate the different flicker values a block chain that is described in IEC61000-4-15 is displayed in Figure 2.11 [15]. A tool that uses this process to evaluate flicker is usually referred to as a flicker meter [15]. In the figure the second and third block represents the lamp-eye-brain model [15]. Because humans are more sensitive in the 8-12 Hz range these frequencies are more heavily weighted [15]. The flicker meters minimum necessary outputs are P_{inst}, P_{st} and P_{lt} [15].

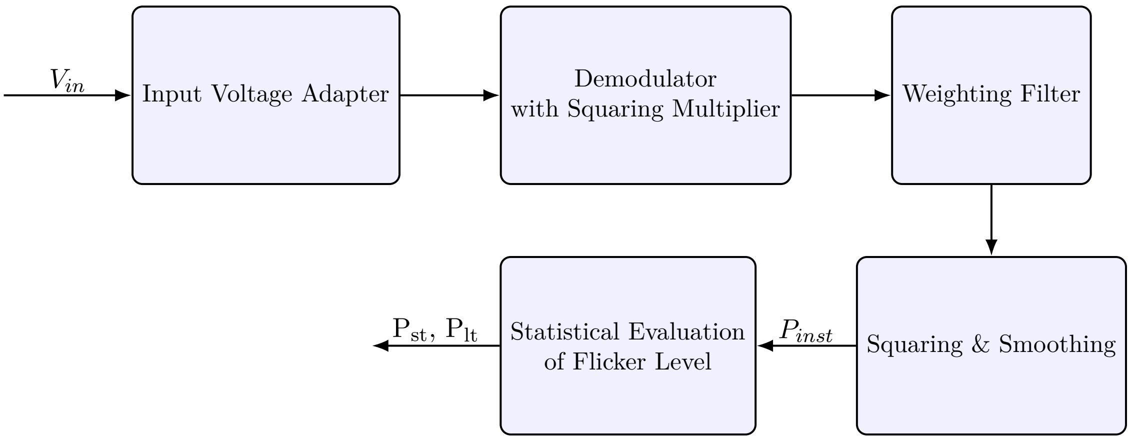

Figure 2.11: Block diagram of flicker measurement chain

2.2.1.1 Flickermeter Test Specifications

In accordance with IEC61000-4-15 all flicker meters must be checked for sinusoidal and rectangular voltage changes [15]. The standard states that certain combinations of voltage fluctuations $\triangle U/U$ and amplitude modulation frequencies f should generate a maximum instantaneous flicker value $P_{inst,max}$ that equals 1 with no more than 8% deviation at the output of block 4 in Figure 2.11 [15]. For testing, mandatory tests are shown in Table 2.3 and Table 2.4 for the case of 230 V, 50 Hz [15].

f [Hz]	$\frac{\triangle U}{U}$ [%]
0.5	0.509
3.5	0.342
8.8	0.196
18.0	0.446
21.5	0.592
25.0	0.764
28.0	0.915
30.5	0.847
33.3	1.671

Table 2.3: Fluctuation frequency and voltage fluctuation for $P_{inst,max} = 1$. Rectangular voltage fluctuations.

f [Hz]	$\frac{\triangle U}{U}$ [%]
0.5	2.325
1.5	1.067
8.8	0.250
20.0	0.704
25.0	1.037
33.3	2.128

Table 2.4: Fluctuation frequency and voltage fluctuation for $P_{inst,max} = 1$. Sinusoidal voltage fluctuations.

2.2.2 Harmonics, interharmonics and sequence components

Harmonics are oscillations that are multiples of the fundamental frequency. In a 50 Hz system the second, third and fourth harmonics have a frequency of 100, 150, 200 Hz and so on. Harmonics appear in the power system due to non-linear loads. Interharmonics is the rest of the frequency spectrum that is not a integer value of h.

Different standards exist to estimate harmonics. In the standard IEC61000-3-6 harmonics are calculated by first defining all current and voltage sources and then all elements in the circuit with frequency dependent behavior [16]. Then each harmonic is injected and the harmonic current and voltage at any node can be calculated.

In the standard IEC61000-4-7 signals from EMT simulations are analyzed [17]. An fast Fourier transform (FFT) is calculated from a moving 200 ms window which is used to calculate the frequency spectrum. Due to the fact that the FFT is performed over a 200 ms moving window on a moving signal the energy of a harmonic will spread out over adjacent frequencies. To ensure a more accurate representation of each harmonic they are calculated in harmonic subgroups. Each harmonic subgroup is 10 Hz large. For example, the first harmonic subgroup is between $45 < f < 55$ Hz. Interharmonics are also calculated in subgroups. Therefore, the interharmonic will be a 45 Hz large window. For example, the first interharmonic will be between $55 < f < 95$ Hz.

2.2.3 Symmetrical components

When a three phase system is unbalanced a one phase equivalent can no longer be used to analyze it [13]. Symmetrical components can instead be used to analysis the unbalanced three-phase systems [13]. In equation (2.24), a three phase voltage can be transformed into 3 symmetrical components that are uncoupled from each other using the Fortescue matrix where a is a 120° counterclockwise rotation [13]. The three components are the positive V_1, negative V_2 and zero V_0 component [13]. The positive component rotates counterclockwise, the negative clockwise and the zero-sequence is a stationary component as displayed in Figure 2.12 [13]. Similarly, currents can be transformed according to equation (2.25) [13]. The impedance matrix can be derived according to equation (2.26) where $\mathbf{A}$ is the Fortescue matrix [13].

$$\begin{bmatrix} V_0 \\ V_1 \\ V_2 \end{bmatrix} = \frac{1}{3} \begin{bmatrix} 1 & 1 & 1 \\ 1 & a & a^2 \\ 1 & a^2 & a \end{bmatrix} \begin{bmatrix} V_a \\ V_b \\ V_c \end{bmatrix} \tag{2.24}$$

$$\begin{bmatrix} I_0 \\ I_1 \\ I_2 \end{bmatrix} = \frac{1}{3} \begin{bmatrix} 1 & 1 & 1 \\ 1 & a & a^2 \\ 1 & a^2 & a \end{bmatrix} \begin{bmatrix} I_a \\ I_b \\ I_c \end{bmatrix} \tag{2.25}$$

$$\begin{aligned} \mathbf{V}_{abc} &= \mathbf{Z}_{abc}\mathbf{I}_{abc} \\ \mathbf{A}\mathbf{V}_{012} &= \mathbf{Z}_{abc}\mathbf{A}\mathbf{I}_{012} \\ \mathbf{V}_{012} &= \mathbf{A}^{-1}\mathbf{Z}_{abc}\mathbf{A}\mathbf{I}_{012} \\ \Rightarrow \quad \mathbf{Z}_{012} &= \mathbf{A}^{-1}\mathbf{Z}_{abc}\mathbf{A} \end{aligned} \tag{2.26}$$

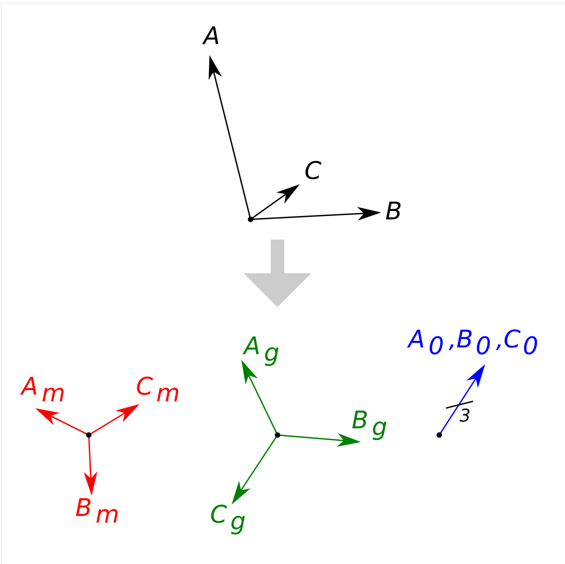

Figure 2.12: Symmetrical components of a three phase system. From [18].

As the zero-sequence current needs a ground connection to flow deliberate grounding can force the current to stay in a certain part of a three phase system [13]. With a two winding transformer Dy connection a zero-sequence current will only flow on the y side if the neutral is grounded as displayed in Table 2.5 [13]. With a Dd connection a ground connection is never established and therefore a zero-sequence can never flow [13]. With a Yy connection a zero-sequence current can only flow through if both sides are grounded [13]. If one side is ungrounded the zero-sequence current will see an open circuit [13].

Case No	**Transformer Connection type**	**Zero-sequence connection**
1	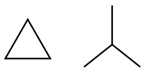	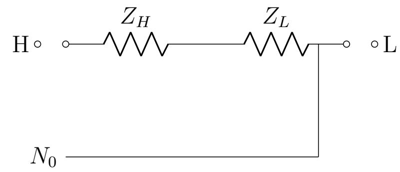
2	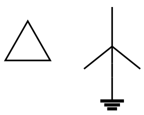	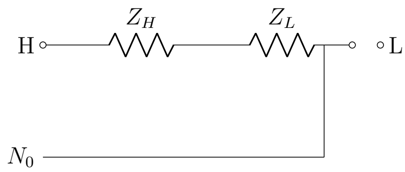
3	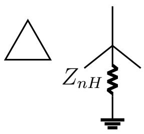	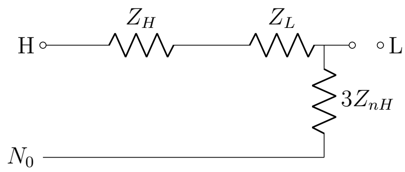
4	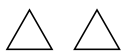	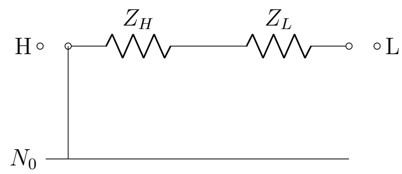
5	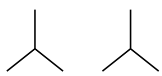	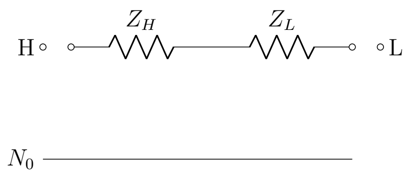
6	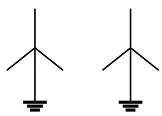	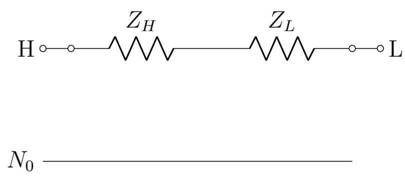
7	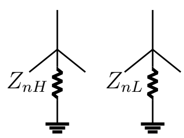	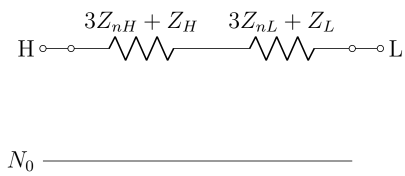

Table 2.5: Comparison of zero-sequences for different types of transformer winding connections.

2.2.4 TSO Power Quality Requirements

The Swedish TSO Svenska kraftnät (SVK) uses the standards IEC61000-3-6 [16] and IEC61000-3-7 [19] for the planning levels of voltage harmonics and flicker [20]. Planning levels are what a TSO wants the future maximum power quality disturbance to be at the connection points to the high voltage (HV) grid [20]. The planning level must always have margins for future connections and changes, therefore the allowed disturbance level for a new installation is usually much lower as displayed in Figure 2.13 [20]. The grid operators such as Vattenfall Eldistribution AB also limit the amount of reactive power that can be exchanged with the grid by adding a cost to each kVAr [21]. The price increase linearly with the amount of reactive power exchanged with the gird [21].

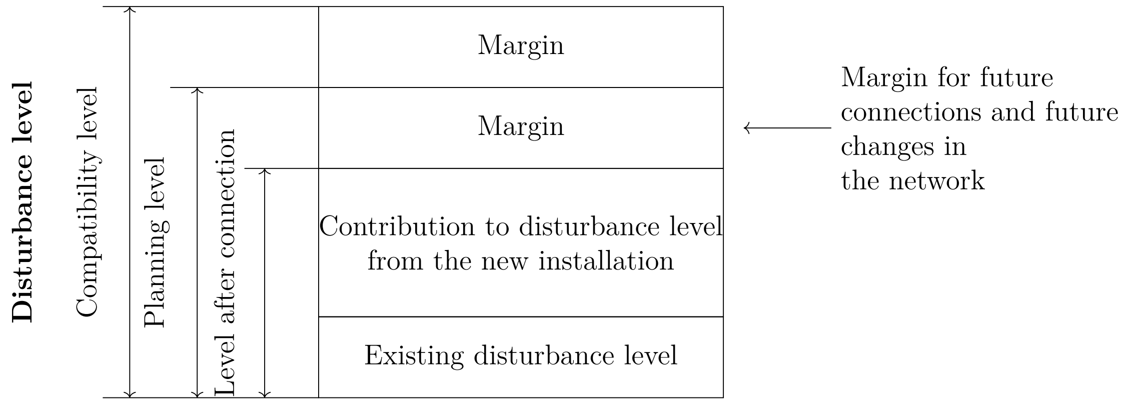

Figure 2.13: Overview of the relationship between compatibility level, planning level, existing disturbance level, and the contribution to the disturbance level from a newly connected disturbing installation.

In [16] the recommendations for voltage harmonic planning levels for a HV and extra high voltage (EHV) grid are displayed in Table 2.6.

Table 2.6: Indicative planning levels for harmonic voltages (in percent of the fundamental voltage) in HV and EHV power systems

Odd harmonics non-multiple of 3		**Odd harmonics multiple of 3**		**Even harmonics**	
h	HV–EHV (%)	h	HV–EHV (%)	h	HV–EHV (%)
5	2	3	2	2	1.4
7	2	9	1	4	0.8
11	1.5	15	0.3	6	0.4
13	1.5	21	0.2	8	0.4
$17 \leq h \leq 49$	$1.2 \cdot \frac{17}{h}$	$21 < h \leq 45$	0.2	$10 \leq h \leq 50$	$0.19 \cdot \frac{10}{h} + 0.16$

IEC61000-3-6 also states that a good conservative planning level for voltage interharmonics should be less or equal to 0.1% of the fundamental voltage [16].

The recommended planning level for voltage flicker $P_{st,95\%}$ is set to 0.8 and $P_{lt,95\%}$ at 0.6. This means that the P_{st} and P_{lt} shall not exceed that limit for 95% of the time [19]. Moreover the $P_{st,99\%}$and $P_{lt,99\%}$ should not exceed 1.5 of the 95% value [19].

SvK states that the planning level during each one-week period, 99% of the 10-minute values of the three-phase voltage unbalance shall be less than or equal to 1% [20].

In [16] its stated that the minimum emission limit allowed for flicker requirements is $P_{st,95\%}$ at 0.35 and $P_{lt,95\%}$ at 0.25 for a single installation. For harmonics, inter-harmonics, and unbalances no minimum emission level is set. However, recently the emission limit that SvK sets for new installations has decreased for harmonics, interharmonics and flicker [6].

2.3 STATCOM

Historically, Static Var Compensators (SVC) have been used as compensating devices for EAFs, SVCs manage its current output with thyristor controlled reactors and capacitors (TCRs and TSCs) [9]. However, due to the characteristics of the SVC it is not optimal for EAF flicker and harmonic compensation[9]. As the response of the SVC is limited by the thyristor ignition it has problems reacting and accurately mitigating the fast dynamics [5]. An SVC typically reduce the flicker content by a factor of 2, meaning the system can expect to receive half the flicker [9].

Today, STATCOMs are the most common applications for EAF compensation [9]. The STATCOM is a shunt compensator, like the SVC, but instead uses a voltage source converter (VSC) equipped with IGBT based converters or similar [9]. This technology allows the device to switch without delay, greatly improving response time [5]. In Figure 2.14 a delta configured STATCOM is shown together with each phase leg. Full bridge converters consisting of four transistors and a DC-link capacitor constitutes the cell, which is capable of generating an output voltage $+U_{DC}$, 0 or $-U_{DC}$ which is dependent on the switching pattern [9]. As the cells are modular the output sinusoidal voltage can be refined in incremental steps by increasing the amount of cells [9]. Delta connected STATCOMs are commonly deployed for their ability to provide reactive power for negative-sequence and harmonic current mitigation but also small amounts of active power [9]. This is possible as the DC voltage of each cell can be regulated by the control around a preselected level, allowing small active power compensations that converges to zero across the operation [9].

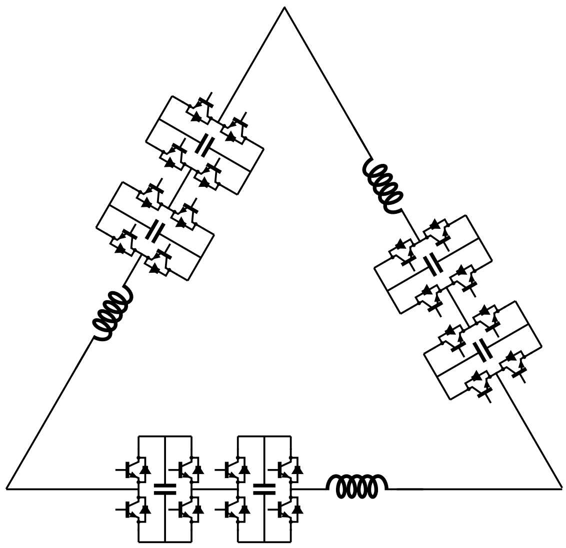

Figure 2.14: Example schematic of delta configured STATCOM.

The dynamic range is also better compared with that of a similarly rated SVC as shown in Figure 2.15. Additionally, a STATCOM can often mitigate low-order harmonics, removing the need for passive filters [9]. This reduces the required size and operational costs of the STATCOM, and if appropriately dimensioned can reduce the flicker values up to 5 times [9].

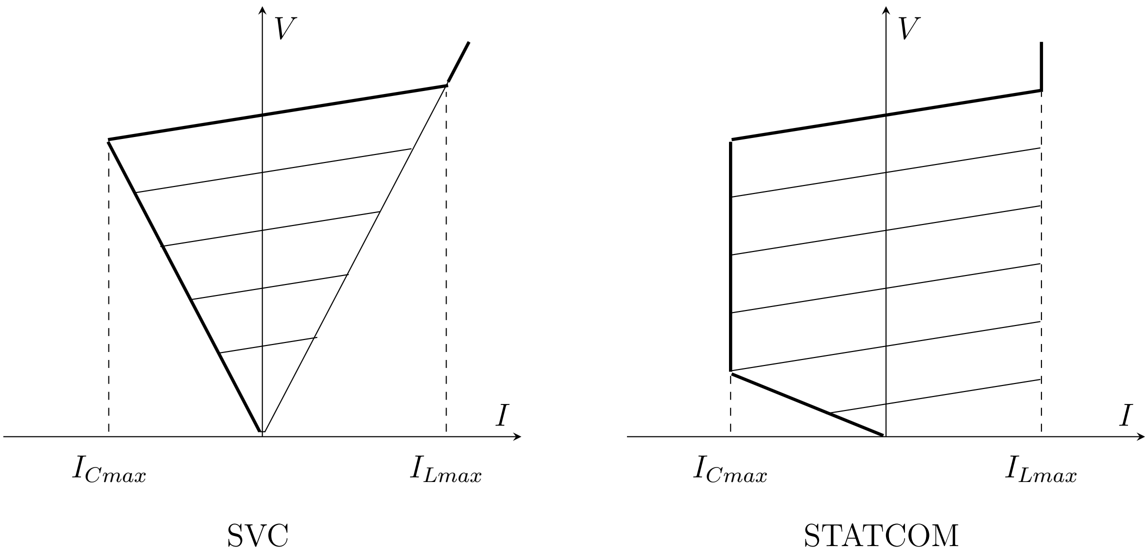

Figure 2.15: Dynamic example performance of SVC and STATCOM.

2.3.1 STATCOM control in EAF application

In a transmission application, the main functional objective of the controller is to manage the bus voltage from disturbances caused by other loads, improving system stability. For the industry EAF application, the objective is instead to manage the disturbances generated by a specific load, in this case the EAF, reducing the variations and flicker seen by the grid [9]. As such, the EAF STATCOM controller uses a dedicated flicker control and PF control with no voltage regulation as shown in Figure 2.16 , usually letting the main step-down transformer manage the dirty bus voltage level if equipped with a tap changer [9].

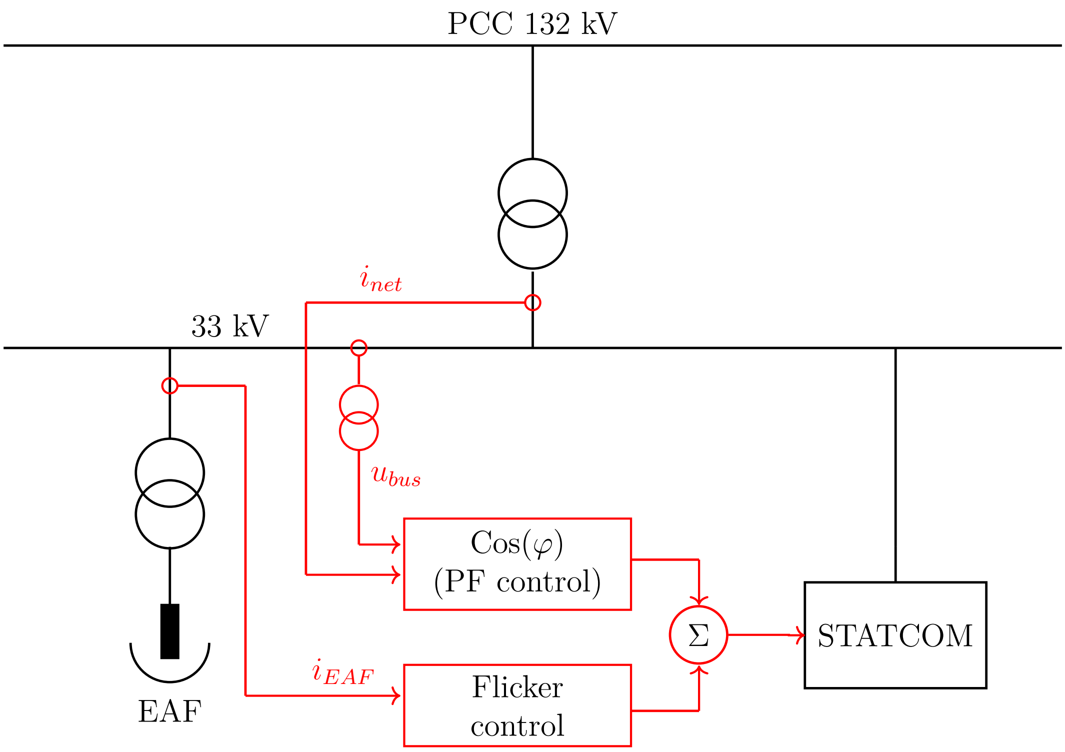

Figure 2.16: Example industry application STATCOM control with dedicated flicker and PF control.

2.3.2 Flicker and Power Factor Control

The flicker controller aims to mitigate all the currents absorbed by the EAF except for the active fundamental component [9]. To achieve this the controller measures the EAF three phase currents i_{EAF} and transforms it to the rotating reference frame using the Clarke ($\alpha\beta$) and Park ($dq0$) transformations, where d and q are the respective active and reactive current contributions. A basic representation of this process is illustrated in Figure 2.17.

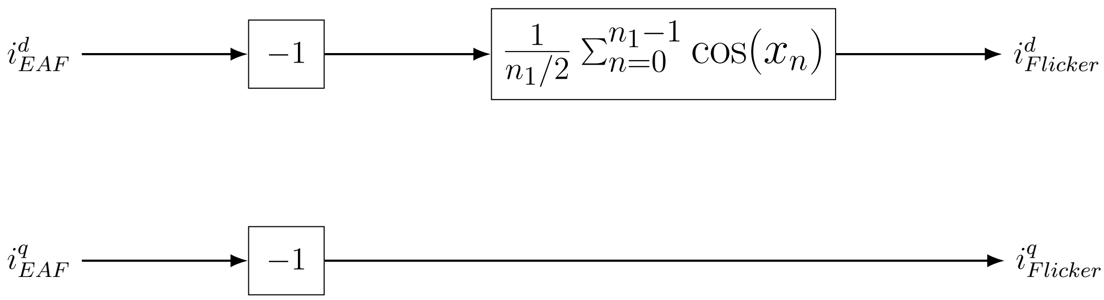

Figure 2.17: Flicker current control block diagram

The flicker controller is designed as an open loop controller as it needs to act fast. i^d_{EAF} and i^q_{EAF} are the EAF active and reactive dq current quantities. As can be seen, i^q_{EAF} only passes through a negative gain block straight to the current controller. i^d_{EAF} also passes through a 2^{nd} order harmonic filter which removes the DC-component. Everything else is sent to the current controller with reversed polarity. The harmonic performance of the controller is highly dependent on the d-current filter used, though a flicker controller can generally provide some harmonic support [10]. More complex filters featuring dedicated harmonic compensation functions require larger converter ratings which in practice means more cells and higher costs [6].

The power factor controller measures the dirty bus voltage u_{bus} and current i_{net} to keep the power factor at a desired value, usually unity, by compensating the reactive power downstream the dirty bus [10]. It is a closed loop controller, deliberately set to be slow compared with the flicker control to not interfere [10].

Due to measurement errors and inherent delays, the response current will naturally not be able to fully mitigate all the variations and flicker. Some effects are also not considered in the model shown in Figure 2.17, such as *dq* cross coupling associated with transients. The Hitachi vMACH controller has filters that consider this, but these cannot be disclosed [6].

2.3.3 Cigré Control

Cigré gives many examples of a STATCOM control in [22]. One of the simpler ones is displayed in figure 2.18. It works by transforming the EAF phase currents to dq currents. To achieve this the voltage phase angle is extracted using a phase locked loop (PLL). Then it averages the dq currents from the EAF over 0.5 seconds to estimate the steady state demands of the furnace. The controller then subtracts the steady state current from the instantaneous current. The magnitude of the difference is then limited to the maximum of the STATCOM current. Finally, the current is transformed to phase current and then input to the dirty bus by the STATCOM to cancel the variation in q and d current by the EAF [22].

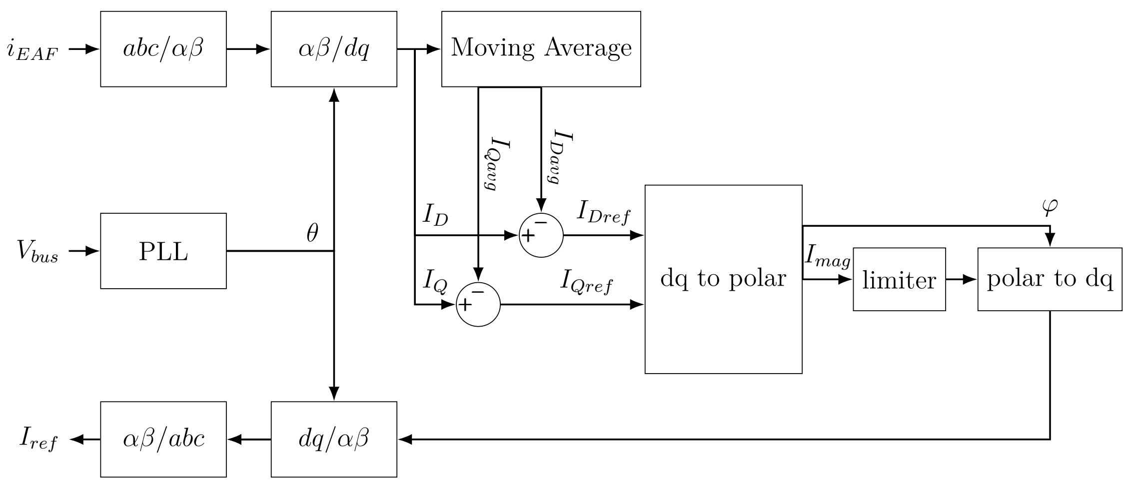

Figure 2.18: Cigré STATCOM controll model.

2.3.4 STATCOM sizing

Figure 2.19 shows an example reactive power response of an EAF compensating STATCOM. The dynamic current capability of the VSC is decisive in the flicker performance of the STATCOM [10]. Apart from maintaining the constant compensation required for the EAF, transformer and other furnaces connected on the bus the VSC needs to have capacity for mitigating the large dynamic current surges drawn by the EAF, even though these may be far in between and short in duration [10]. This is because the $P_{st,95\%}$ and $P_{lt,95\%}$ values are weighted towards higher P_{inst} values [15]. Because of this it is crucial to capture the large dynamic current draw over the entire EAF operation in any models used for STATCOM sizing to be certain that the STATCOM has the right amount of reactive power capability to meet requirements. That is, to allow the right amount of reactive power to fall outside the dynamic operating range. For this aim the bucket EAF is harder to model.

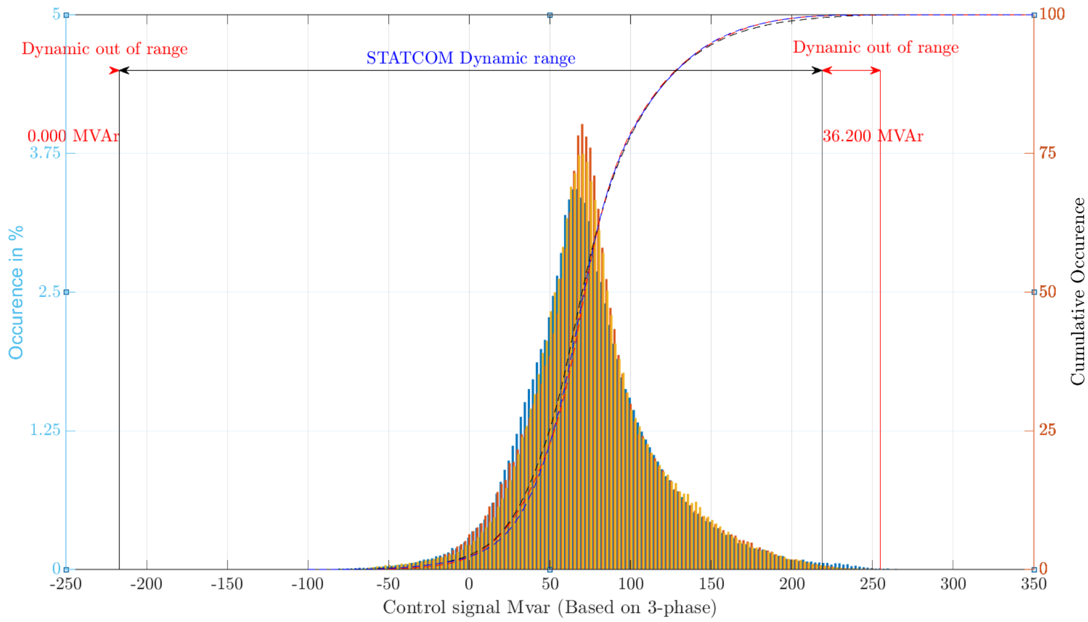

Figure 2.19: STATCOM dynamic range and reactive power injections.

2.4 Step function

A step function is not periodic, so it does not have harmonics in the discrete Fourier series sense [23]. A square wave with a finite rise time will have its continuous harmonic spectra distributed along its DC quantity and cutoff-frequency, as shown in Figure 2.20, determined by the inverse risetime [23]

$$f_{cutoff} = \frac{1}{t_{rise}}$$

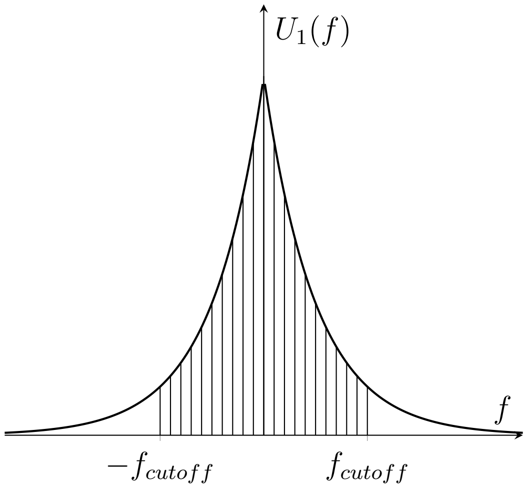

Figure 2.20: Amplitude over frequency of the step function

3
Method

3.1 EAF modeling

The different EAF models considered can be found in Table 3.1. Two flicker models are considered, the EAF measurement and random noise model both mentioned in section 2.1.1. These change how the EAF characteristics are generated. For the random noise model only a voltage-impedance (V/Z) model is considered whereas the EAF measurement model uses a V/Z and current source model. The V/Z model is created to make the EAF measurement model electrically similar to the random noise model to investigate the impact of the source equivalent. Two different EAF measurement files are used with recordings from a bucket charge and consteel EAF. This is done to show the different power quality effects for comparison. The random noise model is tuned to generate similar flicker as the bucket charge EAF. The comparison is made as the bucket charge EAF is more dynamic than the consteel. As such it is more important to compare whether the random model manages to emulate all power quality phenomena of the bucket EAF, should it be used for STATCOM sizing. Lastly, as the thesis aims to compare the detailed vMACH STATCOM controller built in PSCAD with the Cigré controller used in the DPF model all EAF models found in Table 3.1 are implemented in both software to compare STATCOMs and potential software differences. A grid frequency of 50 Hz is used.

Flicker model	EAF Measurement				Random Noise
Source model	V/Z		I		V/Z
EAF type	Bucket	Consteel	Bucket	Consteel	N/A

Table 3.1: All model permutations visualized.

3.1.1 EAF Measurement models

With EAF measurement models, the EAF is represented by an equivalent source that sets the power draw based on measurements from actual EAF operations. This is convenient since the model accurately portrays EAF dynamics without any need for complicated models. The data used is recorded at the primary side of the EAF transformer connecting the EAF to the dirty bus. Because of this the EAF transformer is omitted.

3.1.1.1 Current Source Model

The current source model works by inserting a file with measured phase currents from the EAF. The current in phases A and B is tracked using a PLL. The PLL then reassigns a new time base to lock the signal to a constant 50 Hz, preventing any frequency deviation. The current is then scaled to the right amplitude based on the EAF rated power S_{EAF} and bus voltage. The C phase is generated by subtracting the A and B phases. This step ensures a load without zero-sequence. The EAF is connected to the 33 kV dirty bus through a transformer that is connected to a 4000 MVA grid on the 132 kV side. The grid is displayed in Figure 3.1 and model parameters and ratings are found in Table 3.2. The transformer is grounded on the y side with a 50Ω resistance.

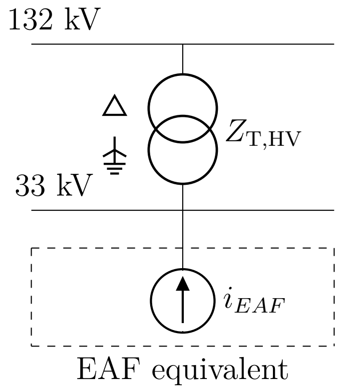

Figure 3.1: Single line diagram of current source model. Without STATCOM.

Parameter	Value	Unit
Grid		
S_{grid}	4000	[MVA]
X/R	10	
T_{HV}	132/33	[kV]
$S_{\text{T,HV}}$	250	[MVA]
$L_{\text{T,HV}}$	0.12	[pu]
$R_{\text{T,HV}}$	0.0025	[pu]
EAF		
S_{EAF}	120	[MVA]

Table 3.2: Current source model parameters.

3.1.1.2 Voltage-Impedance Source Model

The V/Z model is created by replacing the current source with an equivalent voltage source behind an impedance, u_{EAF} and Z_{EAF}, as shown in Figure 3.2.

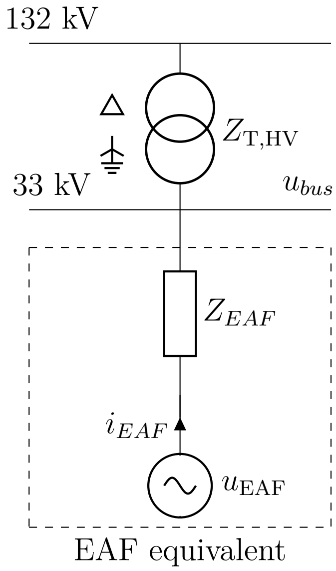

Figure 3.2: Single line diagram of V/Z source model. Without STATCOM.

u_{bus} is the dirty bus phase voltage. With the EAF current measurements, the background phase voltage u_{EAF} can be calculated as

$$u_{EAF} = u_{bus} - Z_{EAF} \cdot i_{EAF}$$

given an arbitrary impedance Z_{EAF}. The impedance is expanded on the form

$$Z_{EAF} = R_{EAF} + sL_{EAF} = R_{EAF}(1 + s\frac{L_{EAF}}{R_{EAF}})$$

which is implemented as a lead-lag filter used to emulate the voltage drop across Z_{EAF} based on the recorded current measurements i_{EAF}.

$$G\frac{1 + sT_1}{1 + sT_2}$$

Here, $T_1 = L_{EAF}/R_{EAF}$ and $G = R_{EAF}$. T_2 is used for noise filtering.

The phase voltage is finally calculated as shown in equation (3.1.1.2).

$$u_{EAF} = u_{bus} - G\frac{1 + sT_1}{1 + sT_2}i_{EAF}$$

As with the current source model, phase A and B are calculated from the measurements and phase C is generated by subtracting A and B. This ensures a load without zero-sequence current.

An X_{EAF}/R_{EAF} ratio of 10 and short circuit capacity SCC of 2 p.u is assumed. R_{EAF} and L_{EAF} can then be calculated as

$$Z_{EAF}^{p.u} = \frac{1}{S_{scc}}$$

$$Z_{base} = \frac{U_{bus}^2}{S_{EAF}}$$

$$R_{EAF}^{p.u} = \frac{Z_{EAF}^{p.u}}{\sqrt{1 + (\frac{X_{EAF}}{R_{EAF}})^2}}$$

$$L_{EAF}^{p.u} = \frac{X}{\omega R} \cdot R_{EAF}^{p.u}$$

$$Z_{EAF} = (R_{EAF}^{p.u} + sL_{EAF}^{p.u})Z_{base} = R_{EAF} + sL_{EAF} \tag{3.1}$$

where ω is the grid angle-frequency. Model parameters and ratings are found in Table 3.3.

Parameter	**Value**	**Unit**
Grid		
S_{grid}	4000	[MVA]
X/R	10	
T_{HV}	132/33	[kV]
$S_{\text{T,HV}}$	250	[MVA]
$L_{\text{T,HV}}$	0.12	[pu]
$R_{\text{T,HV}}$	0.0025	[pu]
EAF		
S_{EAF}	120	[MVA]
L_{EAF}	14.37	[mH]
R_{EAF}	0.451	[Ω]
G	0.451	[Ω]
T_1	31.831	[ms]
T_2	0.250	[ms]

Table 3.3: V/Z model parameters.

3.1.2 Random Noise model

For accurate comparisons of the random noise model with the other models, grid conditions were changed to match the current source model. The 275 kV HV busbar was changed to 132 kV, and the 21 kV busbar was changed to 33 kV, as shown in Figure 3.3.

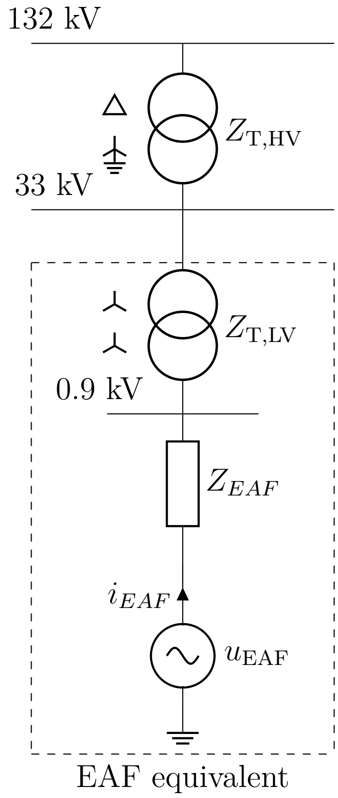

Figure 3.3: Single line diagram of random noise model. Without STATCOM.

The HV transformer was reconfiguration to match the transformer used in the current and V/Z source models. The EAF transformer grounding was lifted. The EAF impedance Z_{EAF} was also changed to make the EAF rated power 120 MVA and power factor ~0.75 upstream of the EAF transformer. This is done as the EAF measurement files are measured at this point. It was calculated by measuring average power and PF over 1 minute simulation runs. The point of common coupling (PCC) at the 132 kV busbar is connected to a grid with a SCC of 4000 MVA. All parameters are found in Table 3.4.

Parameter	Value	Unit
Grid		
S_{grid}	4000	[MVA]
X/R	10	
T_{HV}	132/33	[kV]
$S_{\text{T,HV}}$	250	[MVA]
$L_{\text{T,HV}}$	0.12	[pu]
$R_{\text{T,HV}}$	0.0025	[pu]
T_{LV}	33/0.9	[kV]
$S_{\text{T,LV}}$	120	[MVA]
$L_{\text{T,LV}}$	0.0796	[pu]
$R_{\text{T,LV}}$	0.0025	[pu]
EAF		
S_{EAF}	120	[MVA]
L_{EAF}	10.38	[μH]
R_{EAF}	2.33	[mΩ]

Table 3.4: Random noise model parameters.

To compare the random noise model with the EAF measurement bucket models in terms of flicker levels the white noise is increased by a factor 18 as shown in equation (3.2).

$$k(t) = 1 - 18 \cdot \frac{B \cdot r(t)}{A + B \cdot l_0} \tag{3.2}$$

This is done to meaningfully consider the case with a compensating STATCOM. A factor 18 is chosen as it creates flicker levels comparable with the bucket EAF measurements models. To avoid the current and voltage having different signs due to the large random value a slight modification was done to the original model as displayed in Figure 3.4. To clarify, a few different permutations of the random noise model is evaluated in the results. The original model shown in subsection 2.1.2, the unscaled model without the noise increase, and the scaled random noise model with the noise increase.

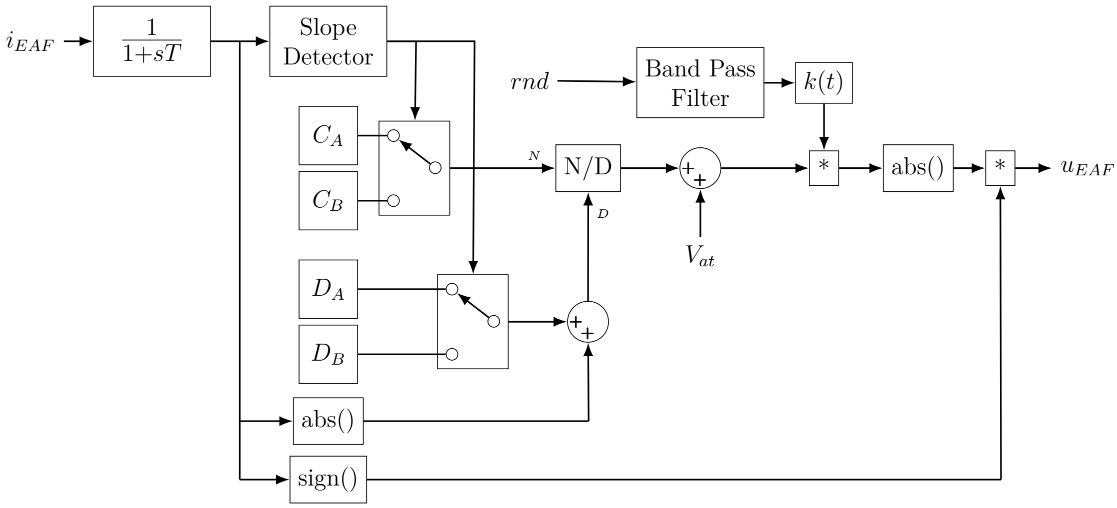

Figure 3.4: Single line modified voltage calculation block diagram. The last two block where added to ensure the correct sign of the voltage.

3.1.3 Implementation in Power Factory

The models described in sections 3.1.1.1 and 3.1.1.2 were implemented similarly in DPF. Electrically the only difference is that the current and voltage sources are grounded in DPF. For the EAF measurement models this is not a problem as they do not have a zero sequence by design. For the random noise model this is mitigated by impedance grounding the transformers therefore removing the zero-sequence current path.

Another difference is that DPF has no PLL to sync the simulated dirty bus voltage with the recorded dirty bus voltage. Because DPF always start the simulated dirty bus voltage at the same phase angle, synchronization could be achieved by delaying the start of the simulation. This is done manually to ensure no phase shift in the dirty buses for the current source model. For the V/Z the phase shift was set to 84.29° to account for the impedances with a X/R ratio of 10.

3.2 STATCOM

All model permutations in Table 3.1 are implemented twice. Once in PSCAD and once in DPF to compare STATCOM models and software. No STATCOM is equipped with energy storage.

3.2.1 PSCAD - vMACH STATCOM

The vMACH is equipped with a power factor control and dedicated flicker control as described in section 2.3.1. The filter used does not feature any dedicated harmonic compensation function, which is done to make the STATCOM control simpler for a better comparison with the Cigré STATCOM. However to show the effect of a dedicated harmonic compensation control a comparison was made on the EAF measurement current source model. Figure 3.5 shows the PSCAD STATCOM connection.

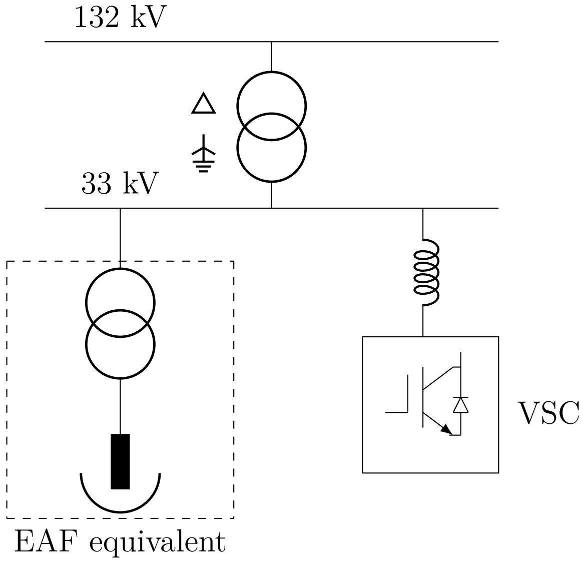

Figure 3.5: PSCAD grid connection with vMACH STATCOM.

The STATCOM is modeled as a delta configured VSC that sets its output current based on the dirty bus voltage and current and EAF current. The STATCOM connection and HV transformer is consistent across PSCAD models, but the EAF equivalent is changed depending on EAF model. The STATCOM is rated at 2200 A and 33 kV.

3.2.2 PowerFactory - Cigré STATCOM

The Cigré STATCOM in DPF is implemented as described in section 2.1.2 but without d current compensation. This was done as tests showed that the average active power produced by the STATCOM did not equal 0. The STATCOM grounding could not be removed as its modeled on a current source block. Figure 3.6 shows the general DPF STATCOM connection.

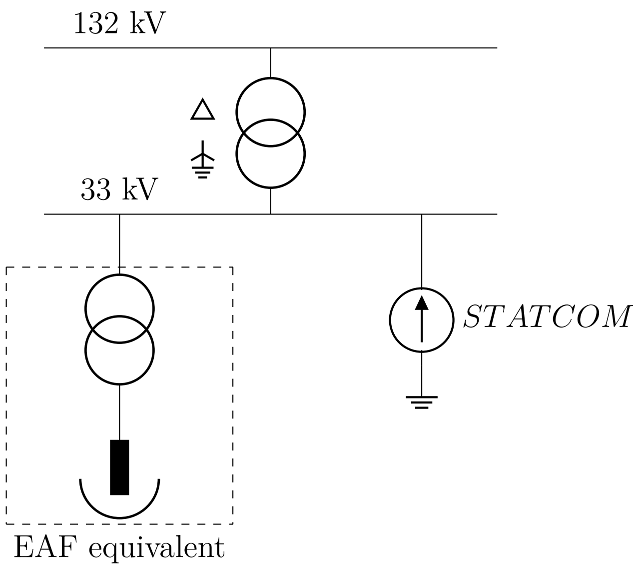

Figure 3.6: DPF grid connection with Cigré STATCOM.

The STATCOM connection and HV transformer is consistent across DPF models, but the EAF equivalent is changed depending on EAF model. The STATCOM is rated at 2200 A and 33 kV.

3.2.3 Step response

To evaluate the different STATCOM model dynamics the step responses are studied. This is done by changing the EAF measurement file with a file containing negative-sequence, active and reactive power steps as shown in Figure 3.7 and Figure 3.8.

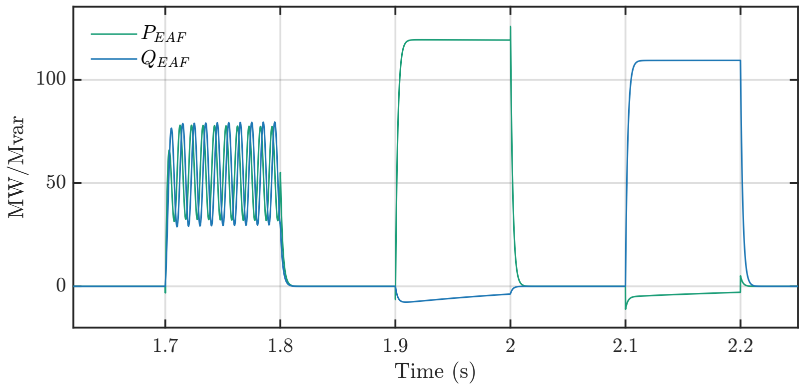

Figure 3.7: Negative-sequence, active and reactive power steps. Shown in that same order. Step length 0.1 s.

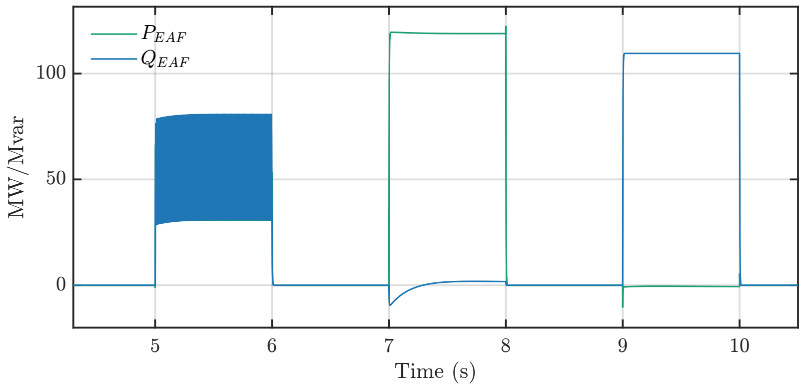

Figure 3.8: Negative-sequence, active and reactive power steps. Shown in that same order. Step length 1 s.

Two different files with different step lengths were used. This was done as some effects of the Cigré STATCOM were not apparent on smaller time scales. Most notably as the controller works by compensating all q-current except the 0.5 s moving average, longer reactive power variations are not mitigated by the STATCOM which was only apparent in the 1 s reactive power step.

3.3 Flicker meter

In DPF a flicker meter is included according to the calculations in [15]. In the settings the flicker meter the user can change sampling rate, initiation time, calculation time for P_{st} and number of samples per P_{lt} value among other settings. The outputs from the flicker meter are P_{st} and P_{lt} values but not P_{inst} values. In the tests performed in this paper the initiation time was set to 10 seconds, and the sampling frequency is the same as the simulation step, 4000 Hz.

In PSCAD an implementation of [15] was built and validated by Hitachi. In the settings the initiation time of the filter is split into two parameters and the nominal voltage frequency of the signal is set. The first initiation time parameter TREL1 sets the time for the rms filter to use nominal voltage as the rms voltage. The second initiation time parameter TREL2 sets the time the rms filter should increase its rms filter speed to reach a steady state value faster. The P_{inst} values is the only output but the P_{st} and P_{lt} values can be calculated in an external script according to the standard [15].

To compare the different flicker meters simulations were made with the unscaled random noise model in DPF with measurements on the 132 and 33 kV phase A voltages. These voltages were then used to evaluate the short time flicker P_{st} across different simulation lengths in DPF. The voltage measurements were also exported to PSCAD for flicker calculation. Results in section 4.1 show that P_{st} values change with simulation time when calculated in DPF but remain constant when calculated with PSCAD. Because of this all flicker related results were calculated with the PSCAD tool. The PSCAD flickermeter was then tested as described in section

2.2.1.1 on square and sinusoidal voltage signals. The signal was created according to equation (3.3) for the square case and equation (3.4) for the sinusoidal case where A is the voltage fluctuation amplitude and f the voltage fluctuation frequency.

$$230 \cdot \sqrt{2}(1 + A \cdot sgn(sin(2\pi f \cdot t)))sin(2\pi 50 \cdot t) \tag{3.3}$$

$$230 \cdot \sqrt{2}(1 + A \cdot sin(2\pi f \cdot t))sin(2\pi 50 \cdot t) \tag{3.4}$$

3.4 Harmonics and Interharmonics measurement

DPF features a built in harmonic tool according on IEC61000-3-6 [16]. This standard does not allow for time domain analysis but only frequency analysis. Therefore, it cannot analyze the signal generated by the EAF models tested in this thesis. DPF has no built in feature to calculate interharmonics.

In PSCAD an implementation of IEC61000-4-7:2002 was built and validated by Hitachi [17]. This allows harmonic and interharmonics to be calculated from any signal. Therefore this tool will be used for all harmonic and interharmonic calculations.

4

Results and Analysis

4.1 Flicker meter

The flicker meters were compared to evaluate their accuracy. As only one P_{st} value per simulation was calculated, $P_{st,100\%}$ will be used instead of $P_{st,95\%}$. Table 4.1 shows resulting $P_{st,100\%}$ values evaluated in PSCAD (P_{st}^{PSCAD}) and DPF (P_{st}^{DPF}) from simulating 1, 5 and 10 minutes in DPF using the unscaled random noise model. Flicker values are based on 132 and 33 kV bus phase A voltages. This was done by exporting the voltage waveforms from DPF and running them as file input to the flicker calculation blocks. For all other results the PSCAD flicker meter was used.

Run time [min]	$P_{st,132kV}^{PSCAD}$	$P_{st,33kV}^{PSCAD}$	$P_{st,132kV}^{DPF}$	$P_{st,33kV}^{DPF}$
1	0.323	0.983	0.320	0.981
5	0.323	0.983	0.322	0.975
10	0.323	0.983	0.322	0.972

Table 4.1: $P_{st,100\%}$ evaluated in DPF and PSCAD on 132 and 33 kV bus for different simulation lengths.

As can be seen the flicker values in DPF decrease on the 33 kV side with simulation length while the 132 kV side increases. As the Random Noise model is used, the flicker should be relatively stable over time considering the model is time independent. Coupled with the lack of insight and control over the flicker meter settings, a decision was made to only use the PSCAD flicker meter.

To make sure the flicker meter was properly tuned all mandatory flicker meter verification tests specified in section 2.2.1.1 were performed. The resulting $P_{inst,max}$ values are shown in Table 4.2 and Table 4.3. Sufficient delay was considered before any measurements to avoid initial transient influence.

f [Hz]	$\frac{\triangle U}{U}$ [%]	$P_{inst,max}$	Deviation [%]
0.5	0.509	1	0
3.5	0.342	1	0
8.8	0.196	1	0
18	0.446	1	0
21.5	0.592	1	0
25	0.764	1	0
28	0.915	1	0
30.5	0.847	1	0
33.3	0.671	1	0

Table 4.2: Input frequency and voltage fluctuation together with recorded P_{inst} values. Rectangular voltage fluctuations.

f [Hz]	$\frac{\triangle U}{U}$ [%]	$P_{inst,max}$	Deviation [%]
0.5	2.325	1	0
1.5	1.067	1	0
8.8	0.250	1	0
20.0	0.704	1	0
25.0	1.037	1	0
33.3	2.128	1	0

Table 4.3: Input frequency and voltage fluctuation together with recorded P_{inst} values. Sinusoidal voltage fluctuations.

4.2 Random noise model

As the random noise model is different from the EAF measurement models with regards to the equivalent circuit and EAF characteristic implementation some tests were specifically done to evaluate factors impacting the flicker. All results are based on 1 minute simulation runs with phase A voltage as input.

4.2.1 Original Model

The original model was found to have zero-sequence current and low power factor, see Figure 4.1 and Figure 4.2.

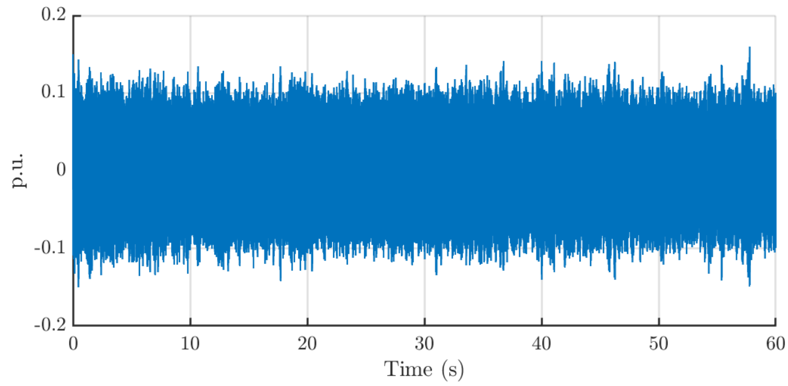

Figure 4.1: Zero-sequence currenton primary side of EAF transformer in the original DPF model

The zero-sequence current appears because the EAF arc voltage and STATCOM are modeled on voltage and current source blocks that are forcibly grounded and connected through YNyn configured transformers with zero grounding resistance. The arc should only pass through the melt between electrodes to protect the furnace shell from current and heat radiation. Transformers are also in reality properly configured to remove any zero-sequence connection. The existence of a zero-sequence in the simulation is then bad because it is unrealistic, but also because the zero-sequence will carry a portion of the flicker content, decreasing the measured flicker upstream the EAF.

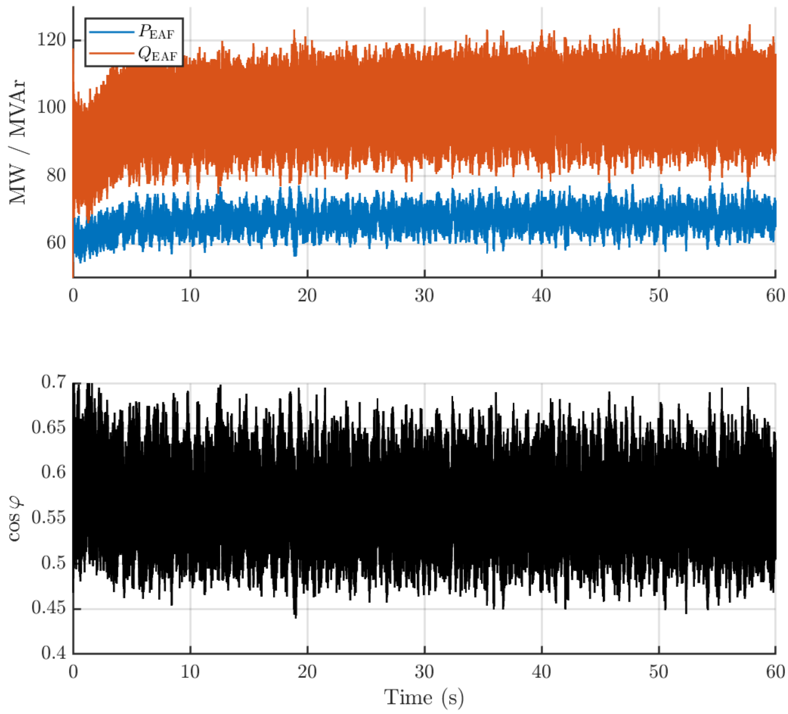

Figure 4.2: Active power, Reactive power and PF on the secondary side of the EAF transformer in the original DPF model.

Figure 4.2 shows that the EAF PF is lower than the operating range of any actual EAF. Observe that the PF plot in Figure 4.2 is measured downstream of the EAF transformer while all other PF results gathered in section 4.4 are measured upstream. As the transformer consumes inductive reactive power the original model has even lower PF upstream. For context Table 4.4 shows the PF effect on the flicker, compared by changing the X/R ratio of the EAF. The scaled random noise model is used as the larger flicker values better shows the effect. Flicker values calculated from phase A voltage on the dirty bus. As can be seen flicker is increased for decreasing PF which is not surprising considering voltage is sensitive to reactive current variations.

X/R ratio	PF	P_{st}
1	0.82	9.347
2	0.7	10.281
3	0.62	10.886

Table 4.4: Power factor effect on flicker.

4.2.2 Transformer grounding

As the EAF and STATCOM grounding could not be lifted in DPF the transformer grounding were studied to evaluate the zero-sequence effects on the flicker. Tests were done with the unscaled random noise model in both PSCAD and DPF to evaluate differing behaviors. Table 4.5 show the resulting $P_{st,100\%}$ values from using different transformer grounding resistances. $R_{g,HV}$ refers to the HV transformer grounding resistance and $R_{g,EAF}$ the EAF transformer grounding resistance. Grounding is always done on both sides of YNyn configuration.

$R_{g,HV}$ [Ω]	$R_{g,EAF}$ [Ω]	**Software**	$P_{st,132kV}$	$P_{st,33kV}$
0	0	PSCAD	0.281	1.026
		DPF	0.347	1.329
	50	PSCAD	0.256	0.787
		DPF	0.323	0.983
50	0	PSCAD	0.260	4.867
		DPF	0.326	5.710
	50	PSCAD	0.256	0.787
		DPF	0.323	0.983

Table 4.5: Short time flicker analysis with varying HV and EAF transformer grounding. $P_{st,100\%}$ calculated on HV and LV side of HV transformer.

Comparing the grounding cases reveals an overall increase in flicker in both software when enabling a zero-sequence path. Whilst the presence of a zero-sequence path does not inherently generate flicker it can increase flicker severity by enabling unbalanced current components to produce additional voltage fluctuations. Particularly when connected to a highly nonlinear load like the EAF. The most extreme case happens for $R_{g,HV} = 50$ and $R_{g,EAF} = 0$ because the zero-sequence current is trapped downstream the HV transformer. The orginal DPF configuration $R_{g,HV} = 0$ and $R_{g,EAF} = 0$ also increase the flicker. Evidently the EAF transformer grounding decides whether or not a zero-sequence path exists.

4.2.3 Random Number Generator in DPF

The different random number generators in DPF were tested. Table 4.6 shows resulting $P_{st,100\%}$ values when using the different random number generators. Unscaled random noise model are used.

Method	$P_{st,HV}$	$P_{st,LV}$
Mersenne twister	0.32	0.98
Linear Congruential	0.39	1.11
Additive Lagged Fibonacci	0.34	1.02

Table 4.6: Short time flicker analysis with varying random number generation method. $P_{st,100\%}$ calculated on HV and LV side of HV transformer.

The three different generators available in DPF all give different flicker values, with a 12.7% increase in flicker between the lowest and highest. In PSCAD an option is not available to choose random number generator method. To make the models as similar as possible the Mersenne twister method was used.

4.3 STATCOM Step Response

Step tests were performed as described in subsection 3.2.3 to gain insight in the controller mechanics.

4.3.1 Active and Reactive Power Response

Figure 4.3 and Figure 4.4 show the measured P and Q step responses for 0.1 and 1 s steps.

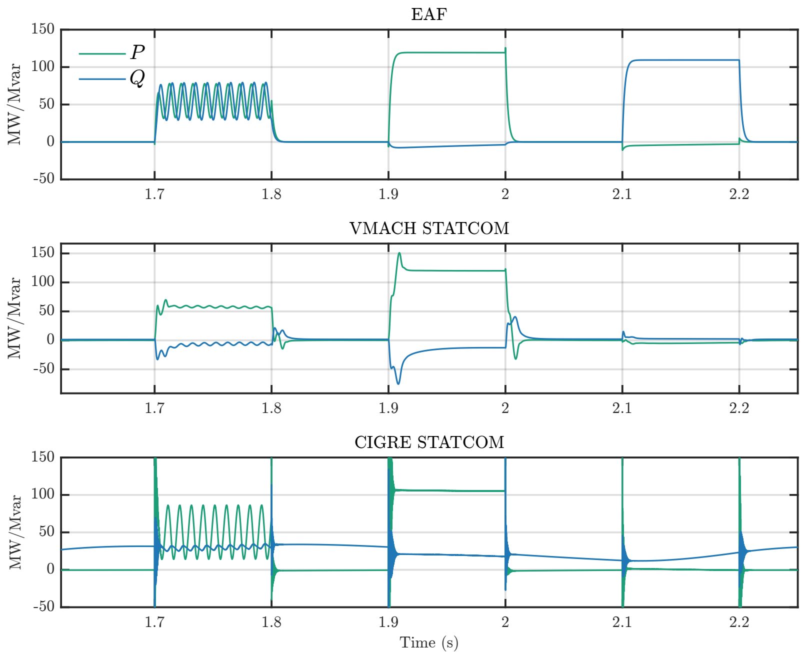

Figure 4.3: Measured dirty bus P and Q responses to negative-sequence, active and reactive power steps at the EAF. Without STATCOM, with vMACH and with Cigré STATCOM. Chronologically in that order. Step length 0.1 s.

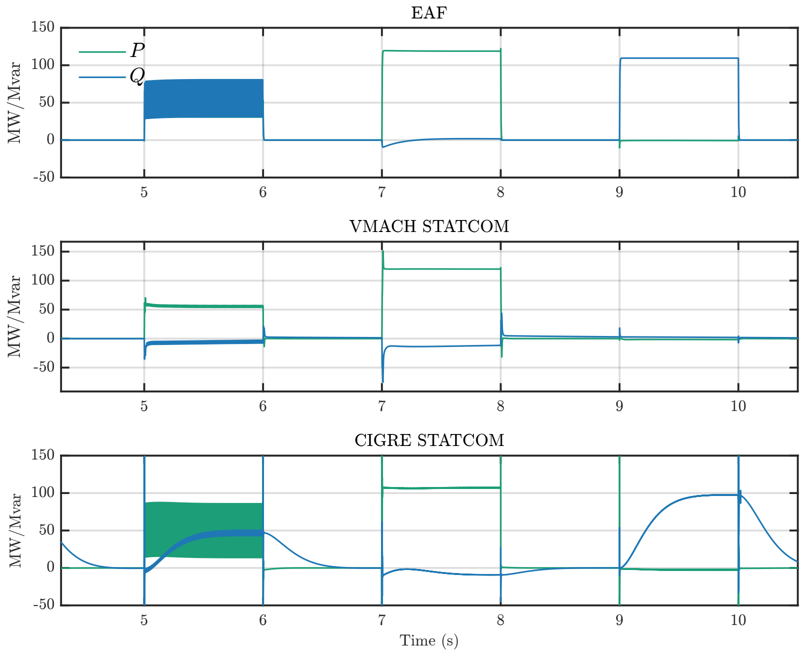

Figure 4.4: Measured dirty bus P and Q responses to negative-sequence, active and reactive power steps at the EAF. Without STATCOM, with vMACH and with Cigré STATCOM. Chronologically in that order. Step length 1 s.

The Cigré STATCOM is limited in its ability to mitigate negative power quality effects for a few reasons. Firstly, the lack of d-current mitigation is evident in the negative-sequence compensation. The negative step response shows that the vMACH outperforms the Cigré controller, which happens because the vMACH flicker controller compensates any non-DC d-current components. The Cigré controller instead disregards all d-current components which can be seen in the step response. Since the reactive power variations is compensated the active power is increased, which leads to larger oscillations as seen during the negative-sequence step in Figure 4.3.

The lack of PF control is also evident. The reactive power step response shows that for any longer change in reactive power output the Cigré STATCOM will stop compensating. This happens because the controller measures the q-current, removes the 0.5 second average and compensates the rest. Because of this the controller does not compensate longer constant reactive power offsets. It only compensates the reactive power variations around the moving average.

Figure 4.5 shows a zoomed window of the STATCOM response transients

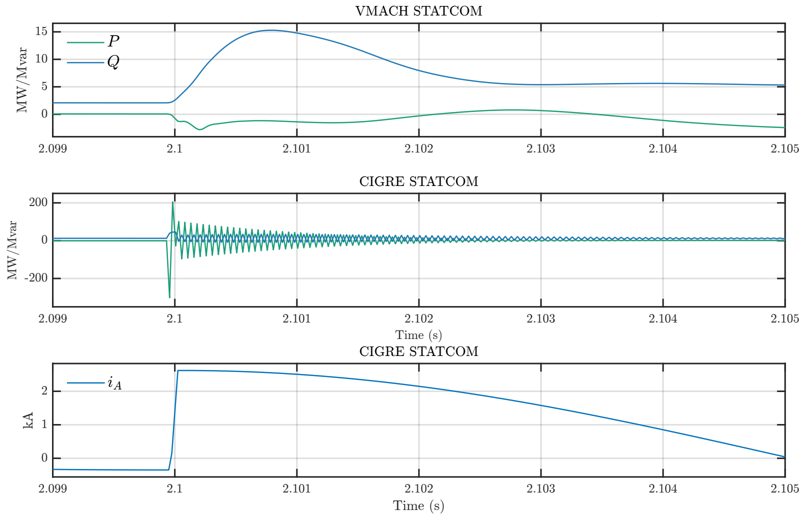

Figure 4.5: Dirty bus P and Q transients during the initial STATCOM reactive power response (top and middle). Cigré STATCOM output phase A current (bottom).

The transient is a oscillation with 20 kHz frequency. It has a sawtooth form since the simulation was done with a 25 μs step size. The initial transient especially affects the active power. As can be seen the response current is set almost immediately by the STATCOM which likely happens as the control lacks any rate of change limiter. As the response is square and has a very short rise time, the harmonic content is very high. The lack of rate of change limiter probably increases the flicker performance of the controller. However, it is a bad representation of an actual STATCOM, which will inherently be limited in its current rate due to the STATCOM reactance.

4.3.2 D-Current Step Response

Figure 4.6 and Figure 4.7 show the d-current response for 0.1 and 1 s steps.

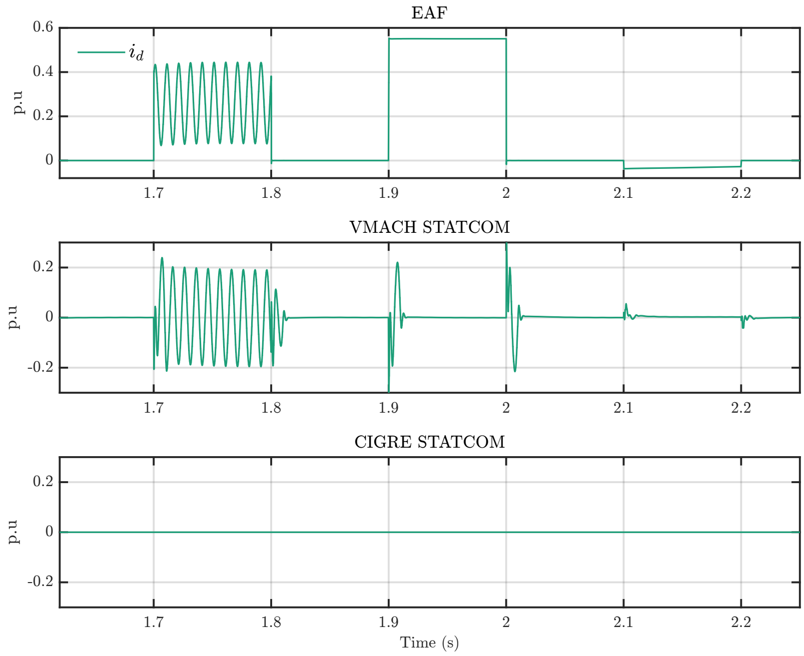

Figure 4.6: vMACH and Cigré STATCOM d-current step response to negative-sequence, active and reactive power steps. Chronologically in that order. Step length 0.1 s.

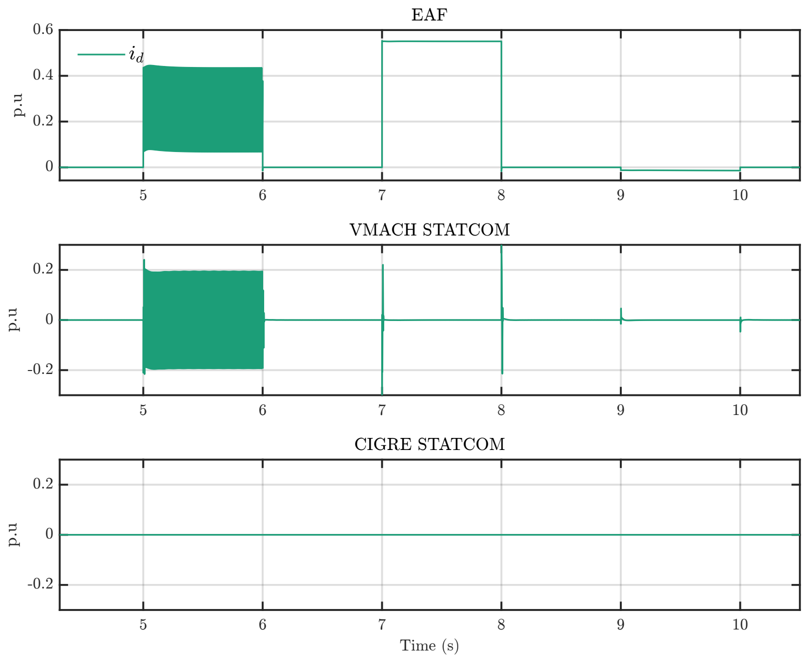

Figure 4.7: vMACH and Cigré STATCOM d-current step response to negative-sequence, active and reactive power steps. Chronologically in that order. Step length 1 s.

As can be seen in the d-current responses the PLL in the Cigré controller is very accurate. This in combination with a lack of a rate of change limiter makes the dq transformation very accurate, allowing it to ignore the d-component entirely.

4.3.3 Q-Current Step Response

Figure 4.8 and Figure 4.9 show the q-current response for 0.1 and 1 s steps.

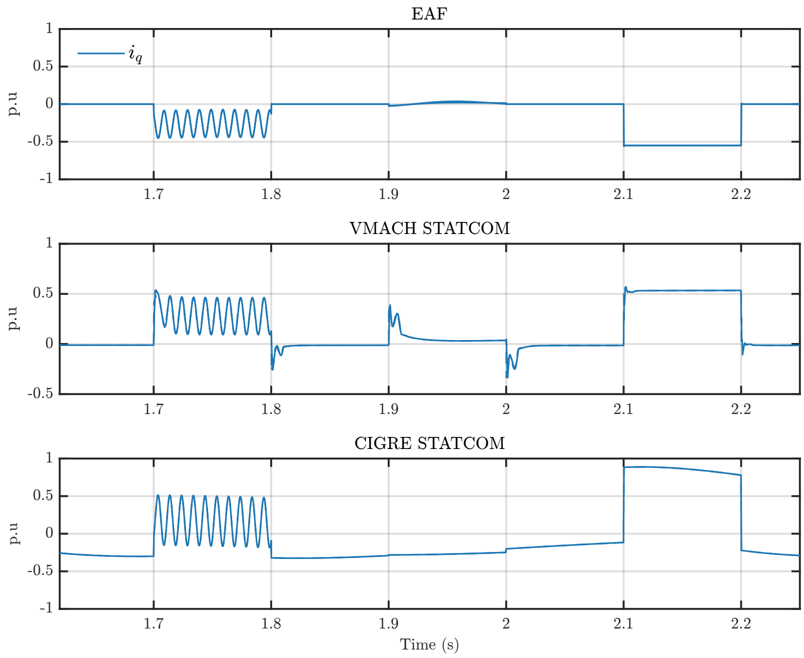

Figure 4.8: vMACH and Cigré STATCOM q-current step response to negative-sequence, active and reactive power steps. Chronologically in that order. Step length 0.1 s.

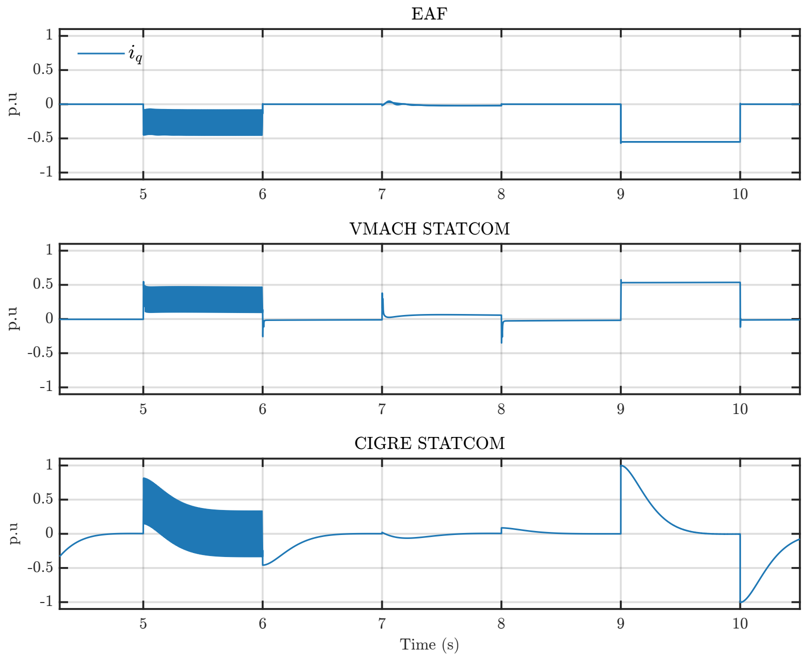

Figure 4.9: vMACH and Cigré STATCOM d-current step response to negative-sequence, active and reactive power steps. Chronologically in that order. Step length 1 s.

In Figure 4.9 it can be seen how the Cigré controllers moving average filter makes the STATCOM supply the bus with reactive power even after the step has ended.

4.4 Simulations

To evaluate and compare the power quality characteristics of the EAF and STATCOM models, 10 minute runs using full waveform EMT simulations were performed in both PSCAD and DPF. For the bucket charge EAFs the recordings are from the boring phase. 25μs solution time step was used. Simulations were made with STATCOM (compensated) and without (uncompensated). Scaled random noise model is used.

4.4.1 Flicker - Overview

Flicker measured according to IEC 61000-4-15 as described in section 2.2.1. The $P_{st,100\%}$ values are calculated on a 10 min time interval. Because of this $P_{lt,100\%}$ values are the same as $P_{st,100\%}$. 132 kV phase A flicker values are shown in Table 4.7 and 33 kV flicker values in Table 4.8.

Flicker model	EAF Measurement								Random Noise	
Source model	V/Z				I				V/Z	
EAF type	Bucket		Consteel		Bucket		Consteel		N/A	
Software	DPF	PSCAD	DPF	PSCAD	DPF	PSCAD	DPF	PSCAD	DPF	PSCAD
Uncompensated $P_{st,100\%}$	3.15	2.74	1.13	1.01	3.53	3.37	1.26	1.22	4.26	3.45
Compensated $P_{st,100\%}$	2.78	0.43	0.98	0.10	1.13	0.45	0.36	0.10	1.09	0.39
Reduction factor	1.30	5.74	1.16	10.10	3.12	7.48	3.50	12.20	3.90	8.90

Table 4.7: Flicker at 132 kV bus, showing $P_{st,100\%}$ for different flicker models. Showing uncompensated values, compensated values and total flicker reduction.

Flicker model	EAF Measurement								Random Noise	
Source model	V/Z				I				V/Z	
EAF type	Bucket		Consteel		Bucket		Consteel		N/A	
Software	DPF	PSCAD	DPF	PSCAD	DPF	PSCAD	DPF	PSCAD	DPF	PSCAD
Uncompensated $P_{st,100\%}$	5.12	8.61	1.32	3.50	10.81	10.54	4.51	4.34	12.42	10.21
Compensated $P_{st,100\%}$	3.73	1.38	1.41	0.28	3.40	1.50	1.03	0.30	3.30	1.28
Reduction factor	1.51	6.24	0.94	12.50	3.18	7.03	4.38	14.67	3.76	8.02

Table 4.8: Flicker at 33 kV bus, showing $P_{st,100\%}$ for different flicker models. Showing uncompensated values, compensated values and total flicker reduction.

For the random noise model and the current source models the DPF simulations result in slightly higher flicker than in PSCAD. The PSCAD V/Z models result in lower flicker, which happens because of the equivalent impedance as it was chosen arbitrarily. It could be modified for more accurate results. The V/Z models in DPF show strange behavior, with higher 132 kV flicker but lower 33 kV flicker than in PSCAD. This would be expected of a system with a ground path, as the excess 132 kV flicker is not seen on the 33 kV side. However, as the HV transformer is Dyn configured there is no ground path to the primary. Unfortunately, the V/Z models in DPF never got running properly during the project. Because of this V/Z models in DPF are a potential source of error. The same can be seen when comparing random and current source models. As measurements on the random noise model show no zero-sequence current on the dirty bus it is unclear why this happens.

Excluding the DPF V/Z models, DPF gives higher flicker values overall. Results for current source models are quite similar, but the random noise model differs more. This is reasonable considering more parameters differ across software for the random models as compared with other models. For example, results in section 4.2.3 show that the random number generator affects flicker outcomes.

The Cigré STATCOM managed to decrease the flicker by an average factor of 3.47 on the 33 kV bus for the bucket charge current and random model. This a low compensation given that a sufficiently sized STATCOM in theory has a reduction factor around 5. As can be seen the performance is much worse for the V/Z models, having an average reduction of 1.18. The vMACH decreased the flicker by an average factor of 7.53 for the bucket charge current and random model and 13.59 for the consteel models.

4.4.2 Flickerspectra

Figure 4.10 shows the 33 kV bus phase A flicker spectra before and after weighting filter for the different models. Flicker spectra refer to the frequency range of the generated flicker. The unweighted spectra are scaled up to match the 8.8 Hz of the weighted curve. Values based on load and network currents. Note that the y-axis are different for the models.

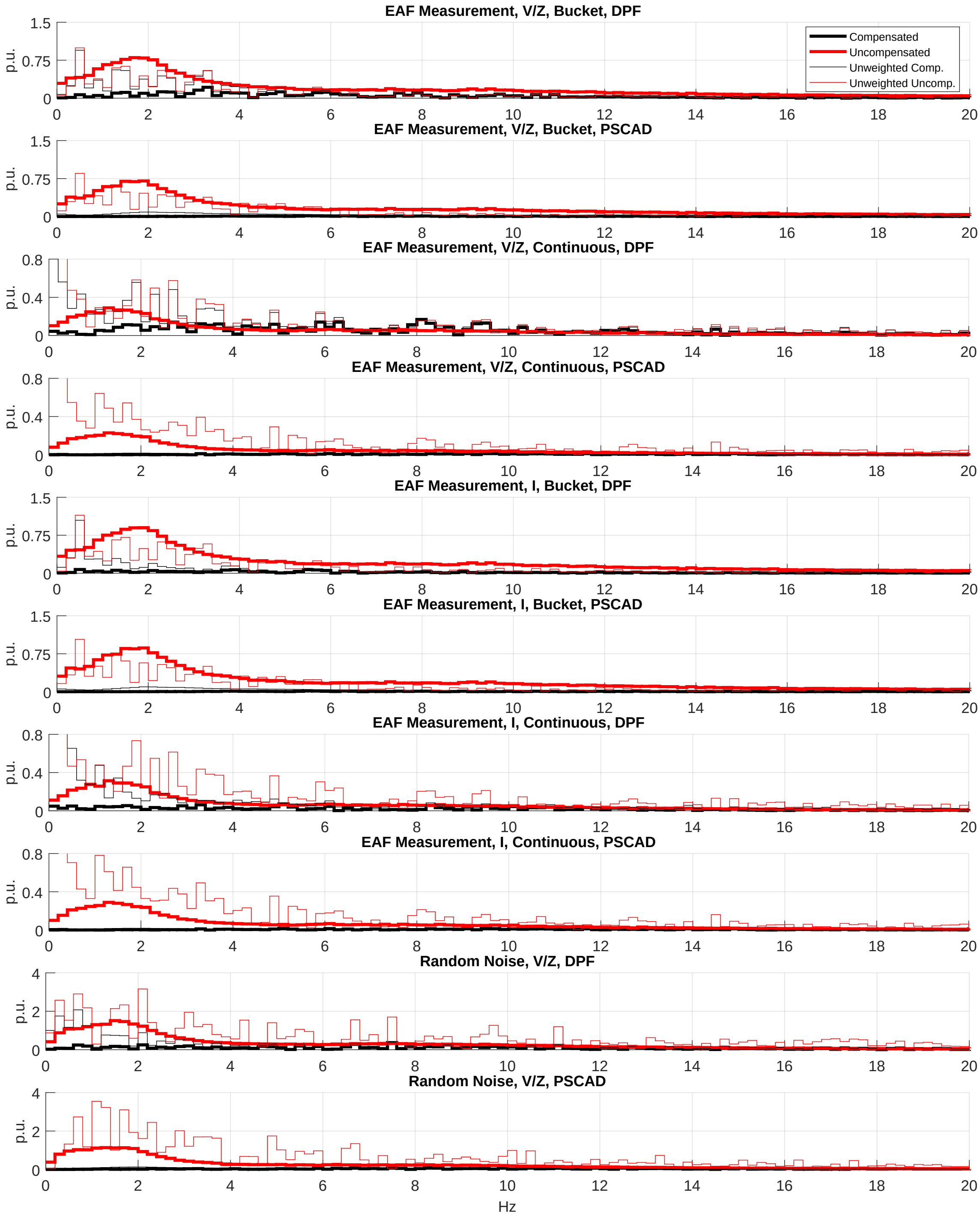

Figure 4.10: Primary bus flicker spectra showing weighted and unweighted values. Compensated and uncompensated values.

For all consteel models the unweighted flicker is concentrated below 1 Hz as shown in Figure 4.11. Magnitudes are similar across consteel models and software. Random noise model is also shown with same y axis as for bucket charge models.

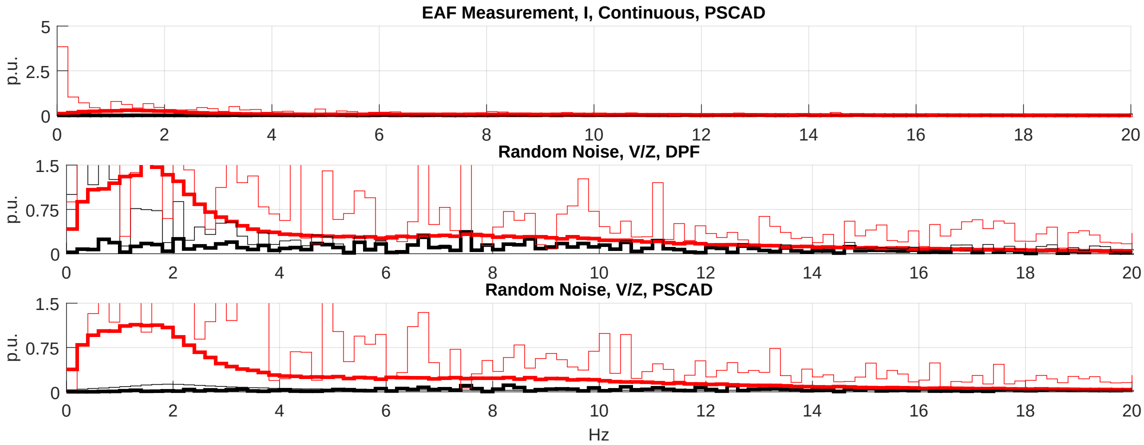

Figure 4.11: Showing peak unweighed flicker for consteel model (top) and weighted flicker for random noise models (middle and bottom).

All EAF measurement models managed to capture their respective furnace weighted flicker range which is a distribution that peaks around 2 Hz. This is typical of EAFs due to the mechanical resonance. The random model fails to capture this behavior and has a squarer shaped flicker with equal intensity from 0.2 to 2 Hz. The unweighted flicker is much bigger than other models in this range. As can be seen the V/Z models in DPF also show similar characteristics to their PSCAD counterparts.

Observing at the black compensated lines, it is also clear that the Cigré STATCOM performs worse than the vMACH. Even though the random model flicker spectra is different the STATCOM performance is still comparable and even somewhat overestimated. For the V/Z DPF model compensation is made around 1-6 Hz, but that it is worse for higher frequencies as compared to any of the other DPF models. Since the flicker is more heavily weighed around 8-12 Hz this affects the compensation more.

4.4.3 Negative-Sequence

Phase A negative-sequence current from EAF and on STATCOM compensated 33 kV bus side. Measured every 200 ms and shown in p.u on the EAF base = 120 MVA.

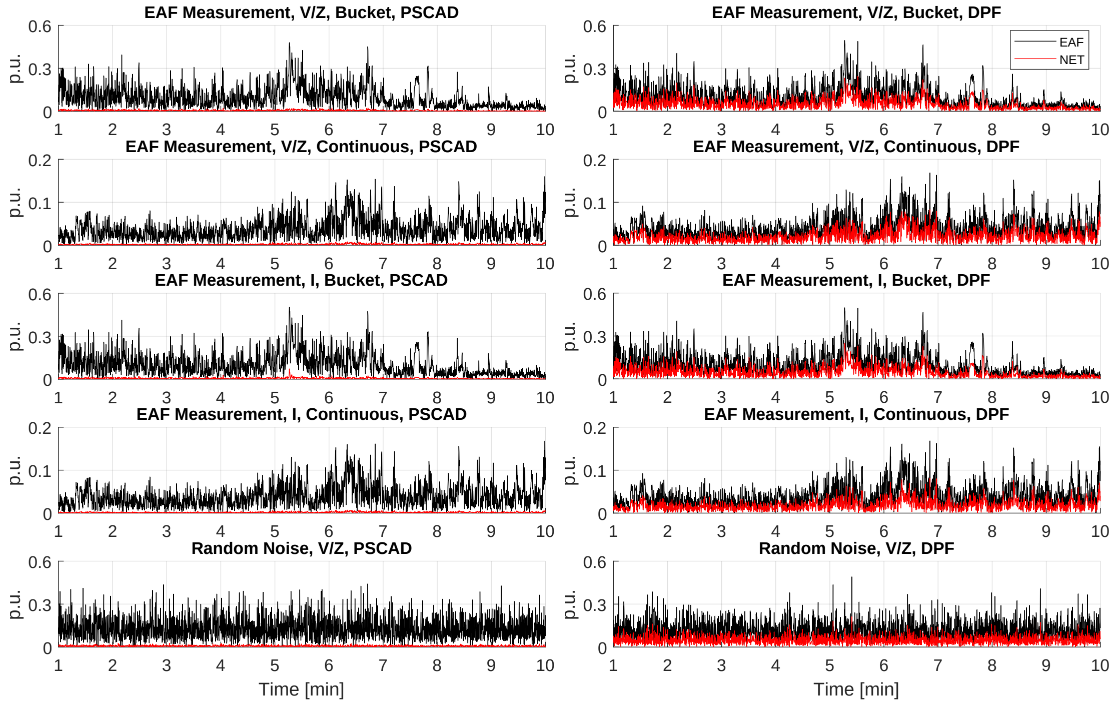

Figure 4.12: Negative-sequence current from EAF and at 33 kV bus. With STATCOM.

The negative-sequence current drawn by the EAFs matched very well across EAF measurement models. The dynamic current is also apparent. For the random model the negative-sequence current peaks are smaller than in the bucket models. It can be seen in bucket models between 5-6 minutes that the NET negative sequence current spikes, which happens as the STATCOM lacks reactive power capability for mitigating this peak. This contributes to the worse STATCOM performance seen in the bucket models compared with the random model.

The red lines show the dirty bus negative-sequence values, which are the compensated values. As can be seen the vMACH decreases the negative-sequence drastically, while the Cigré STATCOM only moderately lowers the negative-sequence. Explanations can again be related to the Cigré controllers disregard of the d-current components, as was seen in section 4.3.

4.4.4 EAF Operation Overview

This section shows the measured EAF current (RMS 20 ms) and the active and reactive power draw across the operation. Figure 4.13 show the dynamic current draw and the P-Q diagram of each model together with a least square assumed P-Q line of each model. This line predicts the short circuit capacity (SSC) of models. Active and reactive power shown as 1 minute average values. Only the compensated PSCAD cases are shown.

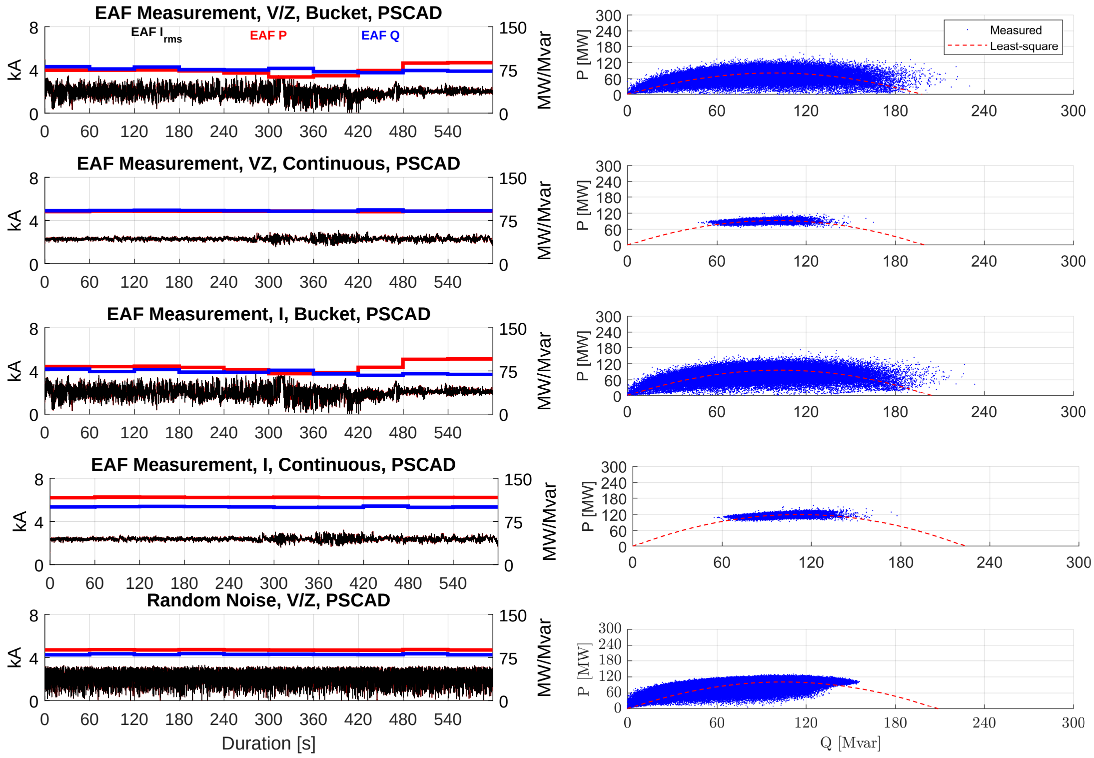

Figure 4.13: EAF Current, Active and Reactive Power for all models in PSCAD (left) together with respective P-Q diagram (right).

Capturing the dynamic current draw is important to accurately capture the flicker generation. For the bucket EAFs the operation is quite varied with currents ranging from 0-4 kA during the worst phases whereas the consteel models are more balanced. As for the negative sequence the random noise model current is generally high and dynamic though it does not reach the current peak seen in the bucket models around 300-360 s. This results in large flicker contribution for the P_{10s} and P_{50s} part of the instant flicker but low contribution for the P_{3s}, P_{1s} and $P_{0.1}$ as shown in Figure 4.14.

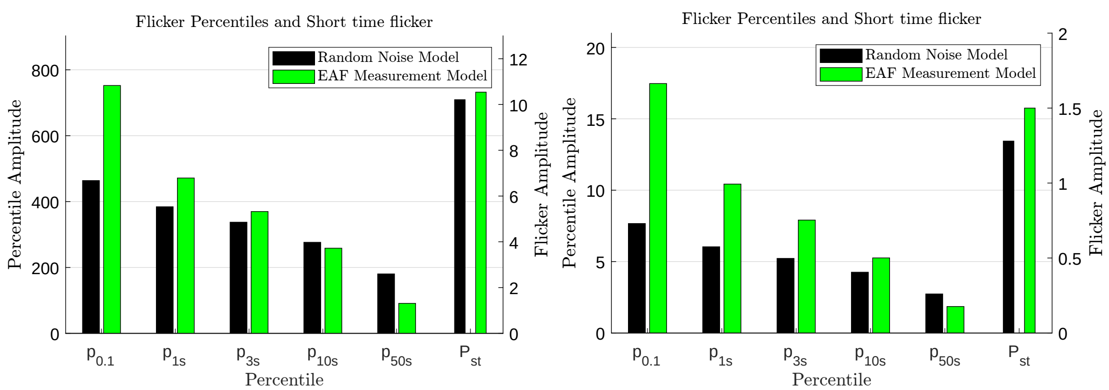

Figure 4.14: Flicker percentile amplitude (left y-axis) and P_{st} amplitude (right y axis) in PSCAD. Uncompensated left. Compensated with vMACH right.

The P-Q diagram shows every operation point throughout the simulation. As can be seen the operation is much more varied for the bucket charge EAF as opposed to the consteel EAF. As can be seen the SCC estimation of the random noise model resembles the current source model, though marginally larger. However the P-Q operating points do not reach the same high active and reactive power values. This is because the EAF impedance, which was used to scale the EAF rating and PF limits the SCC of the grid. The estimated SCC of both V/Z models are decreased compared to the current source models. Figure 4.15 shows the source equivalent and STATCOM impact on the P-Q operating conditions.

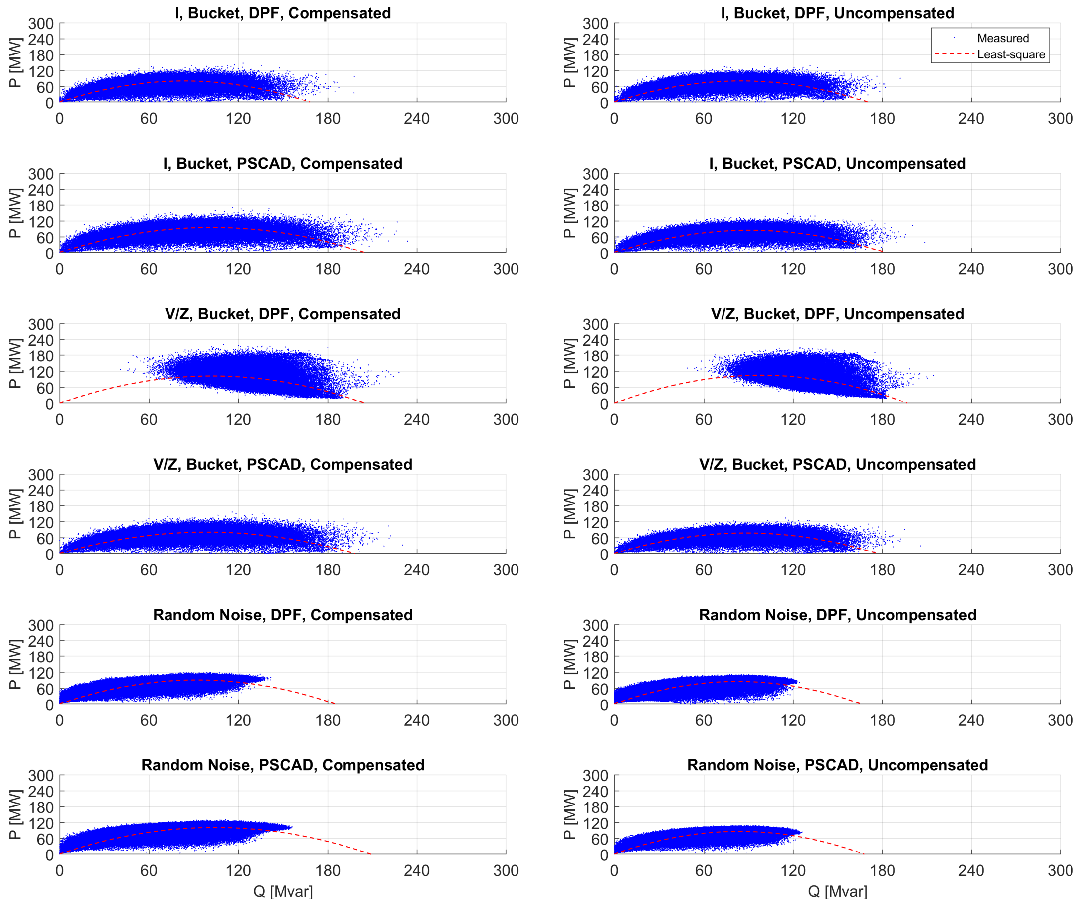

Figure 4.15: P-Q diagrams comparing source and STATCOM model effect on operating conditions.

The abnormality of the DPF V/Z model can be further concluded by its P-Q diagram. For the PSCAD models, the grid is visibly reinforced by the vMACH. As the reactive power variations are compensated, voltage levels at the dirty bus increases which leads to more current and power draw. The Cigré STATCOM has less impact on the grid. Small reinforcements can be seen on the random noise model and marginally on the V/Z model. The difference comes down to worse flicker reduction and lack of PF control.

4.4.5 Harmonic Current Distortion

Figure 4.16 shows the 33 kV phase A uncompensated harmonic and interharmonic distortion of all models. Note that the y-axis are different for the models.

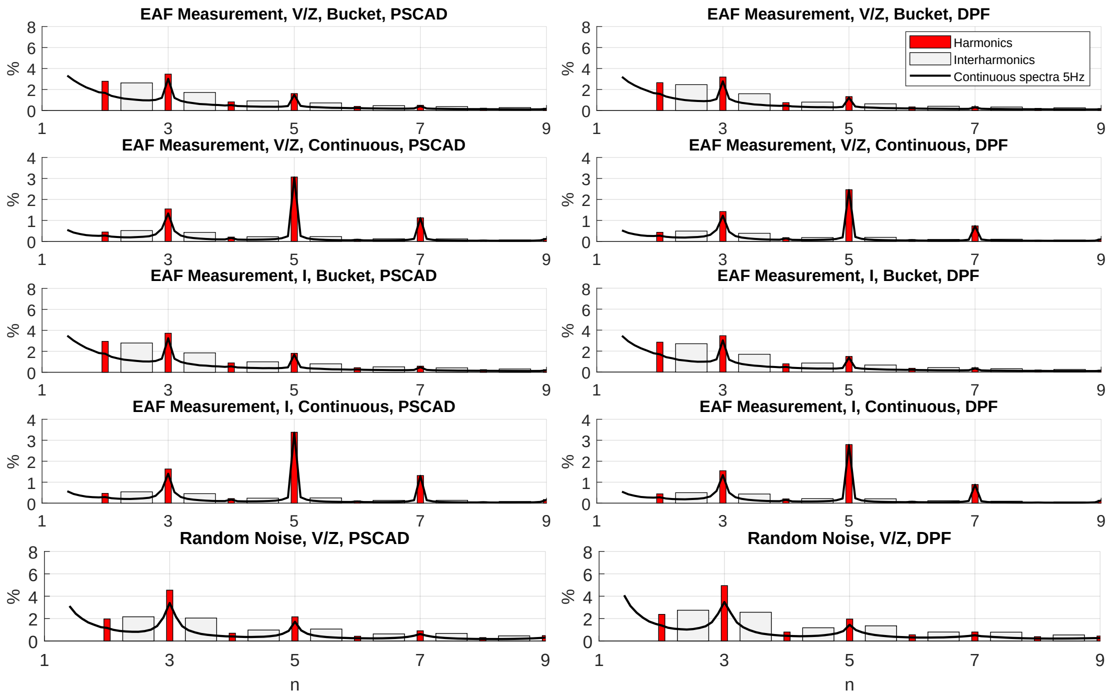

Figure 4.16: 33 kV bus harmonic current distortion in percent of EAF base 120 MVA. Only showing the uncompensated values.

DPF creates lower harmonics for all EAF measurement models. The V/Z models in PSCAD also decreased the harmonics. Overall, the EAF measurement models produced similar harmonics. The random models had a 27.6% lower 2nd and a 30.0% higher 3rd order harmonic compared to the current source bucket models. The mathematical model inherently only generates odd harmonics with the random input distorting the frequencies over the interharmonic spectra, however this does not increase the second harmonic enough.

The interharmonic spectra overall matched well. The main difference is found when comparing the random model to the current source bucket models, having a lower 2nd order interharmonic for the same reason as the 2nd harmonic.

Figure 4.17 shows the compensated harmonic distortion of all models.

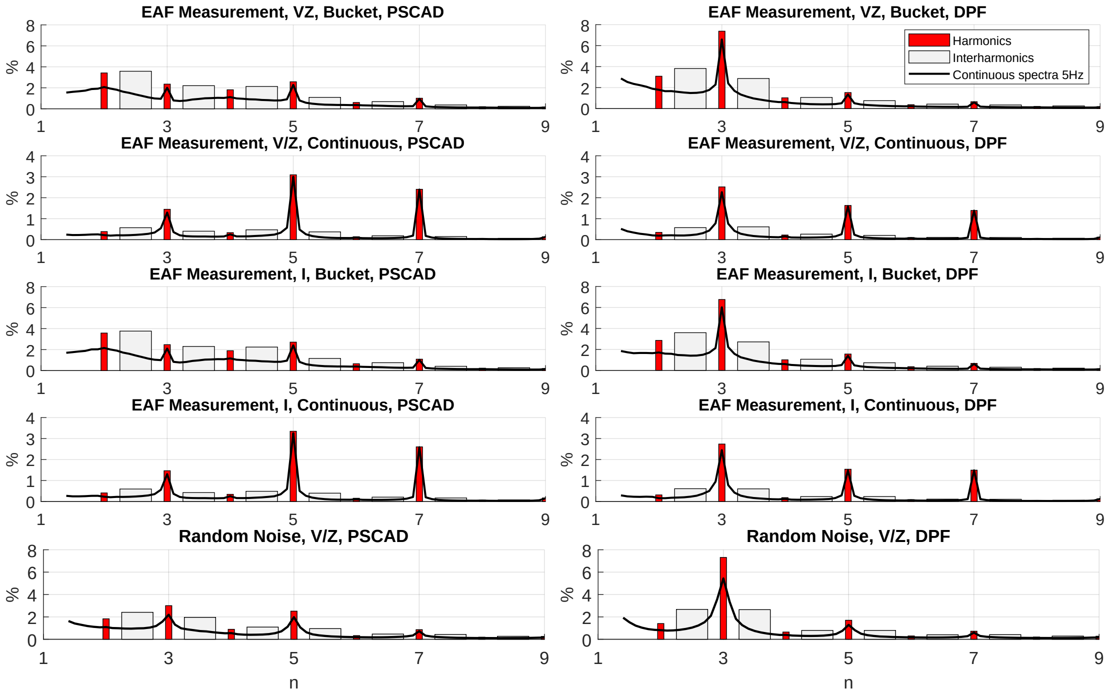

Figure 4.17: 33 kV bus harmonic current distortion in percent of base 120 MVA. Only showing the compensated values.

The vMACH STATCOM increased the bucket current source and random models 2nd harmonic by an average of 9.6% and 5th by 52.8% and decreased the 3rd by an average of 34.4%. For the consteel it decreased the 2nd harmonic by 17.5%, 3rd by 31.3% and increased the 5th by 4.2% and 7th by 86%.

The Cigré STATCOM decreased the bucket current source and random models 2nd harmonic by an average of 14.2%, 5th by 7.6% and increased the 3rd harmonic by an average of 55.4%. For the consteel it decreased the 2nd harmonic by 31.1%, 5th by 40.6%, 7th by 28.6% and increased the 3rd by 36.1%

Table 4.9 shows the total harmonic distortion relative to the EAF current load.

Flicker model	EAF Measurement								Random Noise	
Source model	V/Z				I				V/Z	
EAF type	Bucket		Consteel		Bucket		Consteel		N/A	
Software	DPF	PSCAD	DPF	PSCAD	DPF	PSCAD	DPF	PSCAD	DPF	PSCAD
TDD uncompensated	24.61	24.55	17.80	21.62	26.30	28.66	20.07	23.68	31.43	29.56
TDD compensated	43.29	29.09	19.64	23.55	40.91	30.61	18.38	25.57	41.70	23.81

Table 4.9: Uncompensated and compensated harmonic current TDD on 132 kV bus in ampere.

Observe that the numbers are given in ampere and since the vMACH increases dirty bus voltage the average current in the compensated V/Z models will be slightly higher. The increase of average current will therefore make the proportional changes lower then the absolute ampere values show.

The Cigré STATCOM manages to decrease the consteel current TDD while increasing the other models harmonic TDD. This is due to the high levels of 2nd, 5th and 7th harmonics that it compensates well. Conversely the vMACH increased the consteel current model TDD while decreasing the other models TDD. This is due to the high level of 3rd harmonics that the vMACH compensates well. None of the STATCOM models are supposed to have dedicated harmonic compensation but the Cigré controller performs worse in most models because of high 3rd harmonic injection.

Table 4.10 shows the total harmonic distortion relative to the EAF current load.

Flicker model	EAF Measurement								Random Noise	
Source model	V/Z				I				V/Z	
EAF type	Bucket		Consteel		Bucket		Consteel		N/A	
Software	DPF	PSCAD	DPF	PSCAD	DPF	PSCAD	DPF	PSCAD	DPF	PSCAD
TDD uncompensated	18.0	19.3	4.5	4.5	18.6	20.7	4.3	4.8	20.6	18.6
TDD compensated	26.4	26.2	5.2	5.0	24.8	27.6	4.6	5.2	21.3	18.3

Table 4.10: Uncompensated and compensated interharmonic current TDD on 132 kV bus in ampere.

Uncompensated interharmonic TDD is higher for all models in PSCAD, except for the random noise model. Otherwise TDD matched well. Both the vMACH and Cigré STATCOM increased the TDD of the interharmonics for almost all models. The VMACH and Cigré STATCOMs both increased the TDD by about 16%

4.4.6 Power Factor Overview

Table 4.11 and Table 4.12 shows the average uncompensated and compensated PF values for different system nodes. This is done as EAFs have typical PF operating points which are also related to power quality phenomena.

Flicker model	EAF Measurement								Random Noise	
Source model	V/Z				I				V/Z	
EAF type	Bucket		Consteel		Bucket		Consteel		N/A	
Software	DPF	PSCAD	DPF	PSCAD	DPF	PSCAD	DPF	PSCAD	DPF	PSCAD
Load	0.628	0.702	0.721	0.702	0.760	0.749	0.773	0.758	0.769	0.748
132 kV	0.587	0.676	0.686	0.671	0.732	0.722	0.739	0.721	0.745	0.722

Table 4.11: Power Factor at different system nodes. Uncompensated values.

Flicker model	EAF Measurement								Random Noise	
Source model	V/Z				I				V/Z	
EAF type	Bucket		Consteel		Bucket		Consteel		N/A	
Software	DPF	PSCAD	DPF	PSCAD	DPF	PSCAD	DPF	PSCAD	DPF	PSCAD
Load	0.629	0.702	0.721	0.702	0.760	0.749	0.773	0.758	0.755	0.739
132 kV	0.587	1.000	0.686	1.000	0.730	1.000	0.737	1.000	0.730	1.000

Table 4.12: Power Factor at different system nodes. Compensated values.

A typical EAF has a PF operating point around 0.7-0.9. V/Z DPF models fall outside the realistic operating range. As the impedance used in V/Z models influences the PF further efforts could have been made to make the models similar to the current source models. The uncompensated random noise models have similar PF to the current source models. Moreover, the load PF decreases with the STATCOM which happens because of the grid reinforcement as was seen in Figure 4.15. As the voltage in the EAF measurement V/Z models are calculated based on the current measurements instead of the real time current, the STATCOM does not have the same impact.

As the vMACH features a dedicated PF controller, the PF at the 132 kV is kept at unity. As the Cigré controller lacks a PF controller it does not have any PF influence. This is also seen in the step tests performed in section 4.3. For any long-term change in reactive power the Cigré controller stops compensating.

4.4.7 Cigré STATCOM PQ Compensation

In section 4.4.1 the Cigré STATCOM performance was especially bad for the EAF measurement V/Z models in DPF. To investigate any differences in the reactive power compensation, measurements from the primary bus are plotted in Figure 4.18 and Figure 4.19 for 1 minute simulations.

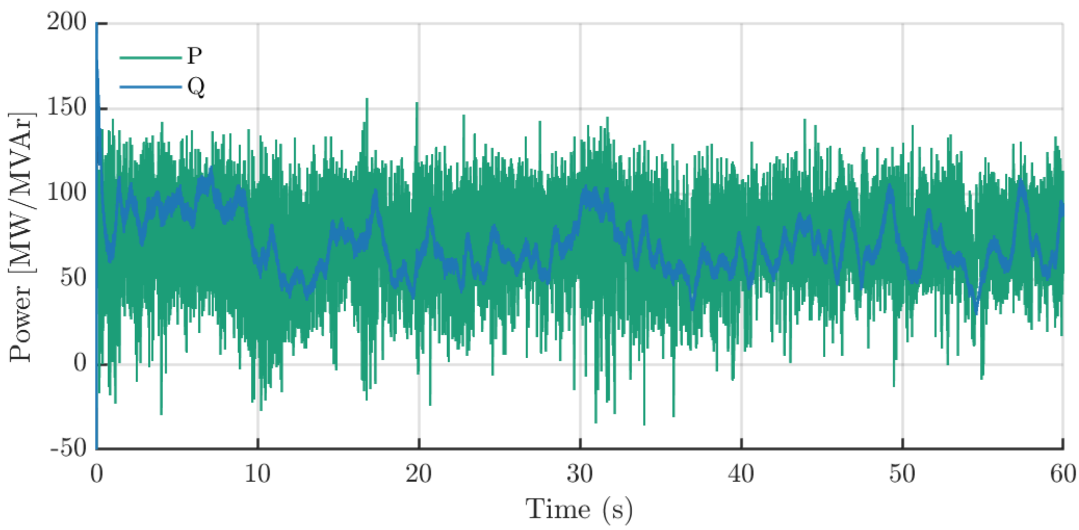

Figure 4.18: Active and reactive power at 132 kV bus I model in DPF.

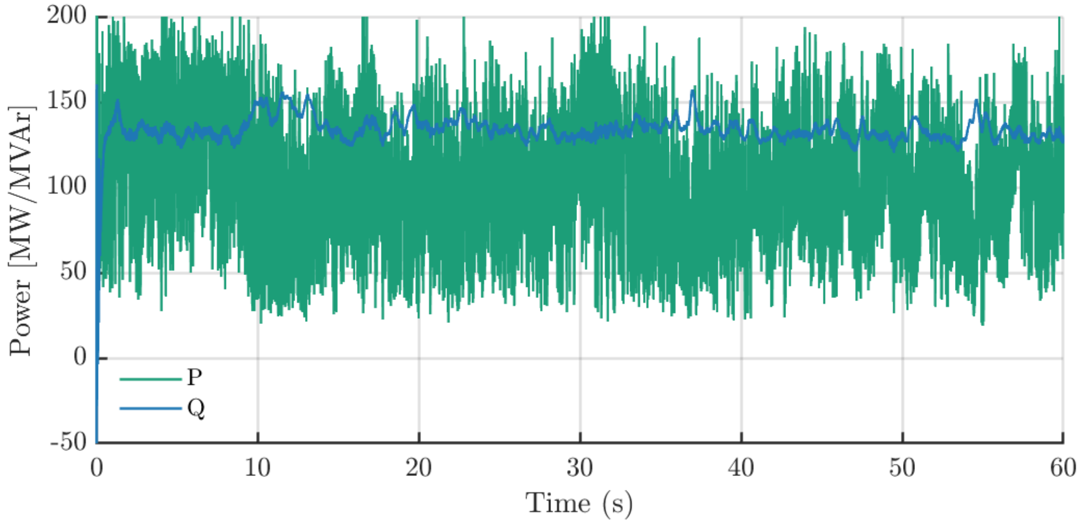

Figure 4.19: Active and reactive power at 132 kV bus V/Z model in DPF.

The figures show that the reactive compensation is similar between the models, therefore the bad V/Z model compensation is not because of a lacking reactive power compensation but more likely due to the flicker spectra generated by the models as was discussed in subsection 4.4.2.

4.4.8 vMACH Harmonic Compensation

Figure 4.20 show a graphic representation of the STATCOM harmonic performance at the 33 kV bus for the model: EAF Measurement, I, Bucket, PSCAD. The graphs show the per harmonic STATCOM compensation in terms of reduction gain. A gain above one means a reduction in the harmonic. Simple vMACH controller shown to the left and the controller with harmonic consideration to the right. Average values of 200 ms above 0.2% of EAF current used.

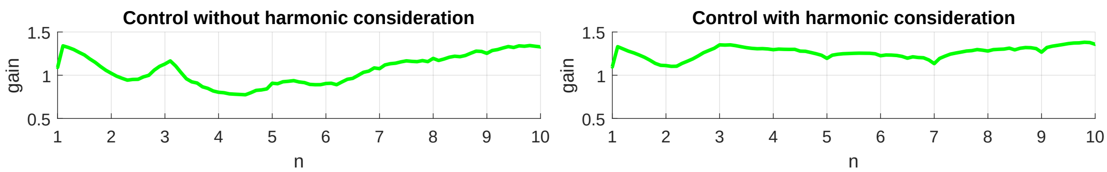

Figure 4.20: vMACH STATCOM harmonic compensation performance with and without harmonic consideration.

It can be seen that the implementation of a more advanced harmonic control model gives better harmonic performance. However, this harmonic compensation adds to the size and cost of the STATCOM as more cells are required.

5
Discussion

5.1 Evaluation of EAF Measurement Models

An advantage of using the current source model with a measurement file is its ease of implementation. The EAF can be changed by changing the input file. However, every EAF is unique and grid conditions, furnace type and other factors will be reflected in the EAF recording. This needs to be considered when using the recordings from a particular EAF for the design of another. For example, the dynamics of a larger EAF cannot be represented by increasing recorded current magnitude. The PF cannot be changed either. When correctly implemented, behaviors that may be difficult or forgotten to implement in a mathematical model can be accurately simulated.

The voltage impedance source model gives the user control of the PF by tuning the X/R ratio. The PF should not be changed too much as the recorded data will reflect the dynamics from the EAF at that given PF. The downside of V/Z model is that the complexity of the simulation increases. Making the model work across different software can be difficult as the lead lag block used is dependent on simulation step-time.

The lack of PLL in DPF models makes the synchronization of the dirty bus difficult. The method used to synchronize manually worked relatively well for the current source models as the difference in PF at the load is low between software. However, for the V/Z model the difference in PF increased as seen in section 4.4.6. Due to the lack of PLL DPF also needs a perfect 50 Hz file. If the frequency deviates slightly for a short period of time the phase angle cannot reestablish itself to the right value. In this thesis a PLL was not implemented in DPF due to time restrictions. However, if DPF is going to be used on a larger scale a PLL would be good to implement to avoid manually synchronizing the simulation and to make the simulation more robust.

When building the voltage model in DPF the program did not allow the grid impedance and arc impedance to be placed inside their respective voltage source as this led to DPF isolating the two parts of the circuit without power flow. It only worked when both impedance blocks were placed outside of the voltage sources. This is weird as both connections are electrically equivalent and could be an underlying source of error.

DPF gave larger flicker values than on the primary side. Harmonic and interharmonics were also found to be lower in DPF, except for the random noise model. This is likely due to some differences in implementation. It is hard to say whether the synchronization method has any effect on these results.

Moreover, the EAF measurement models can not accurately simulate a DC-EAF. This is due to the rectifiers that control the DC current to the EAF. Rectifiers control schemes depend on the dirty bus voltage. When the dirty bus is simulated, it will be different from the recorded voltage, therefore the current will be inaccurate as the rectifiers no longer act on the same voltage. As the measurements are done upstream the rectifiers, a better approach would be to extract the active power from the data. By modeling the rectifiers and inserting the active power on the DC side, this would allow the rectifier control to react to the dirty bus voltage and therefore control the reactive power.

5.2 Evaluation of Random Noise Model

The advantage of the random noise model is that a prerecorded EAF measurement is not needed. However, it requires insight into EAF dynamics and a clear understanding of the type and size of EAF you are trying to emulate. If the random noise model is used for preliminary studies for STATCOM sizing prerequisite knowledge of the flicker levels is required to sufficiently tune the model, similar to what was done in section 4.4. This also requires good knowledge of a specific EAF. Even when flicker levels are comparable with actual values the dynamics are not the same.

As was seen in the negative sequence and EAF operation figures the random model does not emulate the large current peaks found in the bucket model, though it manages to generate similar flicker. This is due to the higher P_{10s} and P_{50s} values that the random model generates. This flicker requires less reactive power capability to compensate compared to the P_{3s}, P_{1s} and P_{01} flicker. To improve this the large current peaks seen in the bucket charge models would need to be better represented, as the flicker contained in this current determines the STATCOM rating. This could be improved by allowing sporadic increases in the apparent power from the EAF or another method of choosing the EAF rating, such as scaling the voltage, since the EAF impedance limits the current draw.

As was determined the flicker spectra generated by the random noise model is different and lacks the 2-5 Hz mechanical resonances. The flicker spectra effects depend on the noise generation method used, the band-pass filter shaping the voltage amplitude modulation. With careful tuning these effects could maybe be improved.

The harmonic content included lower 2nd and higher 3rd order harmonics. This is unrealistic as the 2nd order harmonics are commonly high in EAFs. The 2nd order interharmonics were also low for the random model. These effects depend on the arc voltage equation. It only generates odd harmonics, with the random input spreading the frequencies to the even harmonics, though not enough to be comparable with the measurement model. To improve this an arc model generating even harmonics is needed, or another factor that only generates frequencies around 100 Hz.

The DPF random noise model gave higher flicker and harmonic results compared with the PSCAD model. As discussed, the random number generator method used has a big effect on flicker. However, it cannot be concluded whether this is the only reason for the different flicker values. During the project PSCAD simulations with prebuilt bandpass filters were initially used. When tuned to match the DPF filter these showed big differences in the resulting flicker values which led to a manual implementation of the DPF bandpass filter in PSCAD which improved results. As random number generators are different, the noise formation was likely influenced even with identical filters.

In future studies it would be interesting to test other mathematical EAF models. A natural next step could be using the model in [2] because they use a similar hyperbolic function that could be extended with the exponential function. The problem of not having power variation remains but the exponential function would probably increase flicker and harmonics without scaling the white noise as was done for the random noise model. Switching to the random impedance model in [1] would probably generate similar results to the random noise model as both models were used to generate accurate flicker value but did not focus on any other power quality effect.

5.3 Evaluation of Cigré STATCOM

Comparisons of the Cigré STATCOM with the vMACH show that the Cigré STATCOM makes a less accurate model because of the low reduction factor and harmonic injections. Neither STATCOM model has harmonic compensation, but these injections are still inaccurate as it could be avoided with the vMACH. The lack of PF control is not considerate of requirements considering reactive power consumption from the grid and also means that the Cigré STATCOM can not support the dirty bus voltage like the vMACH.

Admittedly the exclusion of the d-component compensation affects the performance of the STATCOM. Implementing a function that ensures net zero active power use for the Cigré STATCOM would allow for a more accurate comparison with the vMACH STATCOM.

It would be interesting to remove the moving average filter from the reactive power control in the Cigré STATCOM. This could potentially improve the PF of the system, but chances are that the undamped response of the STATCOM would lead to a lot of harmonic injections.

5.4 Public model suitability

The functional objective of any STATCOM sizing is to ensure your facility is grid compliant. Requirements vary between TSOs and are often not given as a flat amount for any EAF connection but tailored based on circumstances. As was explained in section 2.2.4 SvK base their flicker requirements on existing disturbance levels, estimated contributions from the connection and margins for future connections and changes in the network. Requirements for harmonic and interharmonics are treated likewise. Estimated contributions then depend on the size, amount and type of EAFs. As was discussed in section 2.3.4 the large dynamic current variations are the main contributor to the flicker levels of any operation even though they are short in duration. For optimal sizing the STATCOM should be equipped with enough reactive power capability to cover this. It is then important to know the specific requirements, have a good STATCOM model and a sufficient EAF model capable of emulating the characteristics of the physical EAF.

The EAF in the original DPF model has two critical errors. The system grounding that results in a zero-sequence current and a PF that is too low. These factors are important for their impact on the flicker as shown in section 4.2.1. The flicker was improved by increasing the white noise generation. However, this required knowledge of furnace specific flicker levels and as was determined the flicker is more distributed towards high P_{50s} and P_{10s} values instead of the high P_{3s}, P_{1s} and $P_{0.1}$ values that an actual bucket EAF is composed of. As P_{50s} and P_{10s} require less reactive power capability the STATCOM reduction factor is better compared with a bucket EAF. Using this model then risks under-sizing the STATCOM. Furthermore, as the harmonics and interharmonics were different the model is unsuited for any harmonic studies.

The Cigré STATCOM can neither be used for any harmonic studies, and because of the bad flicker reduction factor it is unsuited for any flicker STATCOM study. The performance could be improved by enabling the d-component compensation. Though the d-component control itself should be changed to account for the cell voltage or have some other function to realistically ensure a net zero active compensation for model accuracy. Some additional changes involve removing the moving average filter in the q compensation. This is suggested as the vMACH flicker control compensates all q components, but also as the change can work to improve the dirty bus voltage and PF. A current rate limiter would likely be needed to damp the overshooting current response and to make the response speed more realistic. A dedicated PF control would also help to maintain the bus voltage, though this controller needs to be set slow as to not interfere with the flicker control. These changes are suggested based on the comparison done with the vMACH. It is hard creating accurate model representations without another detailed model for benchmarking, or otherwise experience in the field. STATCOM designs and controls also vary between manufacturers. This needs to be taken into account similarly to how the EAF type affects the study.

5.5 Differences between software

When using PSCAD and DPF, clear differences in their design philosophies become evident. PSCAD does not provide built-in tools for advanced analyses such as flicker or harmonic calculations. Instead, it requires the user to implement such functionality manually, typically through Fortran code. In contrast, DPF aims to offer a more integrated solution, allowing users to design circuits and perform load flow, harmonic, and flicker analyses within a single environment.

Although DPF also supports user-defined implementations through its DIgSILENT Simulation Language (DSL), it provides a wide range of prebuilt components that enable users to avoid extensive coding if desired. These prebuilt tools models make the platform more accessible, particularly for less experienced users. However, this ease of use comes at the cost of reduced flexibility and control compared to PSCAD.

An illustrative example of this difference is the handling of errors, such as the presence of multiple synchronization zones in the V/Z model. In PSCAD, such an issue would likely result in simulation failure or the generation of invalid results. In contrast, DPF attempts to resolve the inconsistency internally by making assumptions about the user's intent, thereby producing a result even in the presence of modeling ambiguities. An experienced DPF user can adapt or reconstruct the provided built-in tools to better suit their specific needs, thereby achieving a level of control comparable to that of an experienced PSCAD user.

Ultimately, both software platforms are designed to perform EMT simulations. Consequently, the primary limitation on the accuracy and reliability of the results is not the software itself, but rather the level of expertise of the user developing the models.

6
Conclusion

The purpose of this thesis was to evaluate whether a publicly available model could be used to reliably study power quality effects related to EAFs and if these results could be used for STATCOM sizing. A mathematical EAF model based on random noise and a simple STATCOM model created by DIgSILENT was compared with an EAF measurement model and a detailed STATCOM. This was evaluated in DPF and PSCAD.

It was shown that the random noise model manages to replicate similar P_{st} values (10.21 in PSCAD, 12.42 in DPF) of the bucket EAF (10.54, 10.81) when tuned accordingly. However, the power quality effects remain misrepresented or lacking context. The model generates the flicker by overemphasizing the amplitude of the P_{50s} and P_{10s} flicker which happens as the model fails to emulate the large current variations seen in the bucket charge models. As the P_{3s}, P_{1s} and $P_{0.1}$ flicker requires more reactive power capability, this results in a better flicker reduction (8.02, 3.76) than the bucket charge EAF (7.03, 3.18). The flicker spectra was found to be uncharacteristic of AC EAFs, having a more uniform distribution instead of the typical 2-5 Hz distribution. The harmonic current most notably contained larger amounts of 3rd and lower amounts of 2nd order harmonics and interharmonics. This is due to the arc voltage equation that does not inherently generate even harmonics but distorts the odd harmonic frequency content with the random noise.

It could be determined that the Cigré model underperforms in its flicker compensation (average 3.47 for bucket EAF) compared with what is generally expected of an EAF application STATCOM, which was exemplified with the vMACH (7.53). The negative-sequence current compensation was also found to be worse than the vMACH. The main reason behind this is the neglect of any non-DC d-component compensation. It was also found that the Cigré increased the 3rd harmonic (average 55.4% for the bucket furnace) while the vMACH increased the 2nd and 5th harmonic (9.6%, 52.8%). However, due to the large 3rd harmonic content in most models the Cigré increased the TDD of all except the consteel models. The interharmonic TDD increased by about 16% for both the Cigré and vMACH models

In conclusion a STATCOM sizing is fundamentally driven by site-specific requirements that depend on existing disturbance levels, expected EAF contributions, and future network margins, that involve significant financial stakes contingent on grid compliance. This requires simultaneous modeling of both flicker and harmonics, as misrepresentation can translate into costly design errors. The random noise model can be tuned to the right flicker value, but the flicker content remains misrepresented. Moreover, as the harmonics and interharmonics are also poorly represented the random noise model can not be used for a STATCOM sizing study. Finally as the Cigré STATCOM performance is much worse than both the theoretical and vMACH STATCOM reduction factor it is also unsuitable for STATCOM sizing.

The DPF models gave slightly higher flicker values and lower harmonic and interharmonic values compared to the models in PSCAD. This can be due to slight differences in models and can not with certainty be attributed to the simulation software. Both DPF and PSCAD are viable simulation tools for simulating EAFs and STATCOMs.

Reference

[1] A. Yazdani, M. L. Crow, and J. Guo, “An improved nonlinear statcom control for electric arc furnace voltage flicker mitigation,” *IEEE Transactions on Power Delivery*, vol. 24, no. 4, ss. 2284–2290, 2009. DOI: 10.1109/TPWRD.2009.2027508.

[2] D. C. Bhonsle and R. B. Kelkar, “Analyzing power quality issues in electric arc furnace by modeling,” *Energy*, vol. 115, ss. 830–839, 2016, ISSN: 0360-5442. DOI: https://doi.org/10.1016/j.energy.2016.09.043. Tillgänglig: https://www.sciencedirect.com/science/article/pii/S0360544216312877.

[3] M. Bejvl, P. Šimek, M. Čerňan, and V. Valouch, “Study of voltage flicker mitigation using emulated electric arc furnace,” *IEEE Transactions on Power Electronics*, vol. 39, no. 7, ss. 8634–8644, 2024. DOI: 10.1109/TPEL.2024.3381430.

[4] G. W. Chang, Y. J. Liu, and C. I. Chen, “Modeling voltage-current characteristics of an electric arc furnace based on actual recorded data: A comparison of classic and advanced models,” in *2008 IEEE Power and Energy Society General Meeting - Conversion and Delivery of Electrical Energy in the 21st Century*, 2008, ss. 1–6. DOI: 10.1109/PES.2008.4596506.

[5] H. Samet and M. A. Jarrahi, “A comparison between svc and statcom in flicker mitigation of electric arc furnace using practical recorded data,” in *2015 30th International Power System Conference (PSC)*, 2015, ss. 300–304. DOI: 10.1109/IPSC.2015.7827763.

[6] J. Rasmussen, private communication, Jan. 2026.

[7] 0x24a537r9, *Electric arc furnace.svg*, https://commons.wikimedia.org/wiki/File:Electric_Arc_Furnace.svg, Wikimedia Commons, Creative Commons Attribution-ShareAlike 3.0; accessed May 19, 2026, 2011.

[8] H. Widmark, *Skrotbaserad processmetallurgi* (Jernkontorets utbildningspaket Del 3). Jernkontoret, 2004.

[9] J. Rasmussen and C.-J. Elm, “Grid-forming control functionality for statcoms in steelmaking applications,” in *AISTech 2023 — Proceedings of the Iron & Steel Technology Conference*, Detroit, MI, USA, May 2023, ss. 2061–2070. DOI: 10.33313/387/232.

[10] J. Rasmussen, T. Bertilsson, and C.-J. Elm, “Grid forming control implementation in a statcom for electrical arc furnace compensation in a uk steel plant,” Göteborg, Sweden, 2023.

[11] H.-J. Odenthal et al., “Review on modeling and simulation of the electric arc furnace (eaf),” *Steel Research International*, vol. 89, no. 1, p. 1 700 098, 2018. DOI: 10.1002/srin.201700098.

[12] Q. G. Reynolds, "The dual-electrode dc arc furnace—modelling brush arc conditions," *Journal of the Southern African Institute of Mining and Metallurgy*, vol. 112, no. 7, ss. 605–611, 2012, [Online; accessed May 19, 2026]. Tillgänglig: http://www.scielo.org.za/scielo.php?script=sci_arttext&pid=S2225-62532012000700004&lng=en.

[13] J. C. Das, *Power System Analysis: Short-Circuit Load Flow and Harmonics*, Second Edition. Boca Raton, FL: CRC Press, 2012, ISBN: 9781439820780. DOI: 10.1201/b11021.

[14] G. Montanari, M. Loggini, A. Cavallini, L. Pitti, and D. Zaninelli, "Arc-furnace model for the study of flicker compensation in electrical networks," *IEEE Transactions on Power Delivery*, vol. 9, no. 4, ss. 2026–2036, 1994. DOI: 10.1109/61.329535.

[15] IEC, *Iec 61000-4-15: Electromagnetic compatibility (emc) – part 4-15: Testing and measurement techniques – flickermeter – functional and design specifications*, Standard, Geneva, Switzerland: International Electrotechnical Commission, Aug. 2010.

[16] IEC, "Electromagnetic compatibility (EMC) – Part 3-6: Limits – Assessment of emission limits for the connection of distorting installations to MV, HV and EHV power systems," International Electrotechnical Commission (IEC), Geneva, Switzerland, IEC/TR 61000-3-6 Edition 2.0, Feb. 2008.

[17] *Electromagnetic compatibility (EMC) – Part 4-7: Testing and measurement techniques – General guide on harmonics and interharmonics measurements and instrumentation, for power supply systems and equipment connected thereto*, Geneva, Switzerland, Aug. 2002.

[18] wdwd, *Symmetrical components three phase*, https://commons.wikimedia.org/wiki/File:Symmetrical_components_three_phase.svg, Accessed: 2026-05-08. Licensed under CC BY-SA 4.0, Aug. 2016.

[19] International Electrotechnical Commission, "Electromagnetic compatibility (emc) – part 3-7: Limits – assessment of emission limits for the connection of fluctuating installations to mv, hv and ehv power systems," International Electrotechnical Commission (IEC), Technical Report IEC/TR 61000-3-7, Feb. 2008.

[20] S. kraftnät, "Teknisk riktlinje elkvalitet tr06, utgåva 1.0," Svenska kraftnät, Tech. Rep., Feb. 2025, Informationsklass K1. [Online]. Tillgänglig: https://www.svk.se/493303/siteassets/aktorsportalen/entreprenorer-i-elnatet/tekniska-riktlinjer/tr06/teknisk-riktlinje-elkvalitet-tr06-utgava-1.0.pdf.

[21] Vattenfall Eldistribution AB, "Tekniska bestämmelser regionnät 2025," Vattenfall Eldistribution AB, Tech. Rep., 2025, Accessed: 2026-05-05. [Online]. Tillgänglig: https://www.vattenfalleldistribution.se/globalassets/2.-foretag/abonnemang-och-avgifter/avtal-och-elnatsavgift/tb-regionnat-2025.pdf.

[22] CIGRÉ Working Group B4.19, "Static synchronous compensator (statcom) for arc furnace and flicker compensation," CIGRÉ Working Group B4.19, Paris, France, Technical Brochure, Sep. 2003, CIGRÉ Study Committee B4.

[23] Y. M. Inshakov, E. B. Solovyeva, and K. S. Ezerov, "Research of the gibbs phenomenon under periodic signals with discontinuities of the first kind on basis of the labviewcomplex," in *2019 International Conference "Quality Management, Transport and Information Security, Information Technologies" (ITQMIS)*, 2019, ss. 502–506. DOI: 10.1109/ITQMIS.2019.8928312.

A

Appendix 1

A.1 Simulations

A.1.1 Harmonic and Interharmonic Overview

Voltage and current harmonics and interharmonics according to IEC 61000-3-6 as described in subsection 2.2.2. The aggregation is performed over a 10 min interval and shows the 95% phase A values

A.1.1.1 Current Harmonics at 132 kV

Current harmonics in Ampere.

Flicker model	EAF Measurement								Random Noise	
Source model	V/Z				I				V/Z	
EAF type	Bucket		Continuous		Bucket		Continuous		N/A	
Software	DPF	PSCAD	DPF	PSCAD	DPF	PSCAD	DPF	PSCAD	DPF	PSCAD
2	16.20	18.44	2.04	2.16	15.45	19.38	1.88	2.26	8.60	9.67
3	38.74	12.86	16.05	7.60	36.40	13.49	14.37	7.69	39.44	15.86
4	5.45	9.67	1.20	1.76	5.30	10.11	0.97	1.80	3.53	4.67
5	8.11	14.35	8.56	18.54	8.19	15.11	9.60	20.33	8.92	13.19
6	1.95	3.23	0.53	0.75	1.85	3.51	0.46	0.81	1.56	1.75
7	3.45	5.36	7.56	12.61	3.53	5.80	7.84	13.67	3.79	4.52
8	1.07	1.06	0.30	0.31	0.91	1.22	0.24	0.35	1.14	1.01
9	0.98	0.89	0.71	0.80	0.84	1.05	0.70	0.95	1.43	1.35
TDD	43.29	29.09	19.64	23.55	40.91	30.61	18.38	25.57	41.70	23.81

Table A.1: Current harmonics 10-min 95%. Compensated values.

Flicker model	EAF Measurement								Random Noise	
Source model	V/Z				I				V/Z	
EAF type	Bucket		Continuous		Bucket		Continuous		N/A	
Software	DPF	PSCAD	DPF	PSCAD	DPF	PSCAD	DPF	PSCAD	DPF	PSCAD
2	14.83	14.71	2.76	2.63	15.54	16.09	2.73	2.74	12.48	10.42
3	17.49	17.59	9.73	10.61	18.85	20.41	10.56	11.19	26.95	24.30
4	4.09	3.98	1.00	1.08	4.31	4.97	1.10	1.16	4.74	3.69
5	7.30	7.31	14.15	17.71	8.23	10.08	16.16	19.51	10.29	11.32
6	1.82	1.77	0.51	0.62	1.96	2.42	0.57	0.69	3.05	2.28
7	2.03	1.98	4.13	6.25	2.32	3.22	4.95	7.34	4.3	4.81
8	1.05	1.09	0.36	0.35	1.12	1.36	0.29	0.39	2.15	1.64
9	0.95	0.98	0.72	1.00	1.06	1.39	0.87	1.25	2.36	2.54
TDD	24.61	24.55	17.80	21.62	26.30	28.66	20.07	23.68	31.43	29.56

Table A.2: Current harmonics 10-min 95%. Uncompensated values.

A.1.1.2 Current Interharmonics at 132 kV

Current interharmonics in Ampere.

Flicker model	EAF Measurement								Random Noise	
Source model	V/Z				I				V/Z	
EAF type	Bucket		Continuous		Bucket		Continuous		N/A	
Software	DPF	PSCAD	DPF	PSCAD	DPF	PSCAD	DPF	PSCAD	DPF	PSCAD
2	20.1	19.0	3.3	2.9	19.1	20.0	3.1	3.0	14.6	12.6
3	15.3	11.9	3.4	2.2	14.0	12.4	2.9	2.3	13.9	10.3
4	5.6	11.5	1.4	2.4	5.5	12.1	1.2	2.5	4.3	5.7
5	4.0	5.8	1.2	1.9	3.7	6.2	1.1	2.0	4.0	5.0
6	2.2	3.6	0.5	1.0	2.0	4.0	0.6	1.1	2.0	2.4
7	1.8	1.9	0.6	0.8	1.6	2.2	0.5	0.9	2.3	2.2
8	1.3	1.2	0.4	0.4	1.1	1.5	0.3	0.4	1.6	1.4
9	1.1	0.8	0.4	0.3	0.9	1.0	0.2	0.3	1.5	1.3
TDD	26.4	26.2	5.2	5.0	24.8	27.6	4.6	5.2	21.3	18.3

Table A.3: Current interharmonics 10-min 95%. Compensated values.

Flicker model	EAF Measurement								Random Noise	
Source model	V/Z				I				V/Z	
EAF type	Bucket		Continuous		Bucket		Continuous		N/A	
Software	DPF	PSCAD	DPF	PSCAD	DPF	PSCAD	DPF	PSCAD	DPF	PSCAD
2	14.2	14.9	3.2	3.0	14.8	15.8	2.9	3.1	12.5	11.6
3	8.9	9.7	2.4	2.6	9.3	10.5	2.6	2.8	12.8	10.8
4	4.5	5.1	1.3	1.3	4.7	5.6	1.2	1.4	5.5	5.2
5	3.4	4.0	1.1	1.3	3.4	4.5	1.1	1.5	6.3	5.6
6	2.1	2.5	0.6	0.7	2.0	2.9	0.6	0.8	3.4	3.4
7	1.7	2.0	0.7	0.7	1.5	2.3	0.5	0.8	3.6	3.6
8	1.4	1.5	0.5	0.4	1.1	1.7	0.3	0.5	2.2	2.4
9	1.2	1.3	0.4	0.4	0.9	1.5	0.3	0.5	2.4	2.5
TDD	18.0	19.3	4.5	4.5	18.6	20.7	4.3	4.8	20.6	18.6

Table A.4: Current interharmonics 10-min 95%. Uncompensated values.

A.1.1.3 Current Harmonics from EAF

Current harmonics from EAF in % of EAF nominal rating.

Flicker model	EAF Measurement								Random Noise	
Source model	V/Z				I				V/Z	
EAF type	Bucket		Continuous		Bucket		Continuous		N/A	
Software	DPF	PSCAD	DPF	PSCAD	DPF	PSCAD	DPF	PSCAD	DPF	PSCAD
2	2.9	2.9	0.6	0.5	3.0	3.1	0.5	0.5	2.0	2.0
3	3.4	3.6	1.9	2.0	3.6	3.9	2.0	2.1	4.8	4.6
4	0.8	0.9	0.2	0.2	0.8	0.9	0.2	0.2	0.7	0.7
5	1.5	1.7	2.7	3.2	1.6	1.9	2.9	3.6	2.0	2.2
6	0.4	0.4	0.1	0.1	0.3	0.5	0.1	0.1	0.4	0.4
7	0.4	0.5	0.8	1.2	0.4	0.6	0.9	1.4	0.8	0.9
8	0.2	0.2	0.1	0.1	0.2	0.3	0.0	0.1	0.3	0.3
9	0.2	0.2	0.1	0.2	0.2	0.3	0.2	0.2	0.4	0.5

Table A.5: Current harmonics 10-min 95%.

A.1.1.4 Current Interharmonics from EAF

Current interharmonics from EAF in % of EAF nominal rating.

Flicker model	EAF Measurement								Random Noise	
Source model	V/Z				I				V/Z	
EAF type	Bucket		Continuous		Bucket		Continuous		N/A	
Software	DPF	PSCAD	DPF	PSCAD	DPF	PSCAD	DPF	PSCAD	DPF	PSCAD
2	2.8	2.8	0.6	0.6	2.8	3.0	0.6	0.6	2.4	2.2
3	1.7	1.9	0.5	0.5	1.8	2.0	0.5	0.5	2.4	2.1
4	0.9	1.0	0.2	0.2	0.9	1.1	0.2	0.3	1.1	1.0
5	0.7	0.8	0.2	0.3	0.7	0.9	0.2	0.3	1.2	1.1
6	0.4	0.5	0.1	0.1	0.4	0.5	0.1	0.2	0.6	0.6
7	0.3	0.4	0.1	0.1	0.3	0.4	0.1	0.2	0.7	0.7
8	0.3	0.3	0.1	0.1	0.2	0.3	0.1	0.1	0.4	0.5
9	0.2	0.2	0.1	0.1	0.2	0.3	0.0	0.1	0.5	0.5

Table A.6: Current interharmonics 10-min 95%.

A.1.1.5 Voltage Harmonics at 132 kV

Voltage harmonics % of rated voltage.

Flicker model	EAF Measurement								Random Noise	
Source model	V/Z				I				V/Z	
EAF type	Bucket		Continuous		Bucket		Continuous		N/A	
Software	DPF	PSCAD	DPF	PSCAD	DPF	PSCAD	DPF	PSCAD	DPF	PSCAD
2	0.10	0.24	0.05	0.08	0.19	0.25	0.08	0.09	0.10	0.16
3	0.23	0.22	0.10	0.14	0.62	0.23	0.25	0.14	0.68	0.28
4	0.04	0.22	0.02	0.05	0.13	0.23	0.09	0.05	0.0.06	0.11
5	0.06	0.40	0.06	0.51	0.24	0.42	0.31	0.56	0.25	0.38
6	0.02	0.11	0.01	0.03	0.13	0.12	0.13	0.03	0.03	0.06
7	0.03	0.21	0.05	0.51	0.20	0.23	0.34	0.55	0.14	0.18
8	0.02	0.05	0.02	0.02	0.19	0.06	0.23	0.02	0.03	0.04
9	0.02	0.04	0.02	0.04	0.22	0.05	0.25	0.05	0.06	0.07
THD	0.26	0.62	0.14	0.73	0.80	0.65	0.64	0.79	0.75	0.55

Table A.7: Voltage harmonics 10-min 95%. Compensated values.

Flicker model	EAF Measurement								Random Noise	
Source model	V/Z				I				V/Z	
EAF type	Bucket		Continuous		Bucket		Continuous		N/A	
Software	DPF	PSCAD	DPF	PSCAD	DPF	PSCAD	DPF	PSCAD	DPF	PSCAD
2	0.10	0.18	0.05	0.08	0.18	0.21	0.06	0.08	0.12	0.15
3	0.10	0.30	0.06	0.20	0.32	0.35	0.20	0.21	0.43	0.42
4	0.03	0.09	0.02	0.04	0.10	0.11	0.06	0.04	0.07	0.07
5	0.05	0.21	0.10	0.50	0.24	0.29	0.46	0.55	0.29	0.32
6	0.02	0.05	0.01	0.03	0.07	0.08	0.08	0.03	0.06	0.06
7	0.01	0.07	0.03	0.25	0.11	0.12	0.21	0.29	0.15	0.18
8	0.01	0.03	0.01	0.02	0.09	0.05	0.15	0.02	0.06	0.05
9	0.01	0.03	0.01	0.05	0.10	0.06	0.15	0.06	0.10	0.12
THD	0.16	0.42	0.13	0.60	0.48	0.53	0.61	0.66	0.57	0.60

Table A.8: Voltage harmonics 10-min 95%. Uncompensated values.

A.1.1.6 Voltage Interharmonics at 132 kV

Voltage interharmonics % of rated voltage.

Flicker model	EAF Measurement								Random Noise	
Source model	V/Z				I				V/Z	
EAF type	Bucket		Continuous		Bucket		Continuous		N/A	
Software	DPF	PSCAD	DPF	PSCAD	DPF	PSCAD	DPF	PSCAD	DPF	PSCAD
2	0.1	0.3	0.0	0.1	0.3	0.3	0.1	0.01	0.2	0.2
3	0.1	0.3	0.0	0.1	0.3	0.3	0.1	0.1	0.3	0.2
4	0.0	0.3	0.0	0.1	0.1	0.3	0.1	0.1	0.1	0.2
5	0.0	0.2	0.0	0.1	0.1	0.2	0.1	0.1	0.1	0.2
6	0.0	0.1	0.0	0.0	0.1	0.2	0.1	0.0	0.1	0.1
7	0.0	0.1	0.0	0.0	0.1	0.1	0.1	0.0	0.1	0.1
8	0.0	0.1	0.0	0.0	0.2	0.1	0.3	0.0	0.0	0.1
9	0.0	0.0	0.0	0.0	0.1	0.1	0.2	0.0	0.1	0.1

Table A.9: Voltage interharmonics 10-min 95%. Compensated values.

Flicker model	EAF Measurement								Random Noise	
Source model	V/Z				I				V/Z	
EAF type	Bucket		Continuous		Bucket		Continuous		N/A	
Software	DPF	PSCAD	DPF	PSCAD	DPF	PSCAD	DPF	PSCAD	DPF	PSCAD
2	0.1	0.3	0.0	0.1	0.2	0.3	0.1	0.1	0.2	0.2
3	0.1	0.2	0.0	0.1	0.2	0.2	0.1	0.1	0.2	0.2
4	0.0	0.1	0.0	0.0	0.1	0.1	0.1	0.0	0.1	0.1
5	0.0	0.1	0.0	0.0	0.1	0.1	0.1	0.0	0.2	0.2
6	0.0	0.1	0.0	0.0	0.1	0.1	0.1	0.0	0.1	0.1
7	0.0	0.1	0.0	0.0	0.1	0.1	0.1	0.0	0.1	0.1
8	0.0	0.1	0.0	0.0	0.1	0.1	0.2	0.0	0.1	0.1
9	0.0	0.1	0.0	0.0	0.1	0.1	0.1	0.0	0.1	0.1

Table A.10: Voltage interharmonics 10-min 95%. Uncompensated values.

A.1.1.7 Voltage Harmonics at 33 kV

Voltage harmonics % of rated voltage.

Flicker model	EAF Measurement								Random Noise	
Source model	V/Z				I				V/Z	
EAF type	Bucket		Continuous		Bucket		Continuous		N/A	
Software	DPF	PSCAD	DPF	PSCAD	DPF	PSCAD	DPF	PSCAD	DPF	PSCAD
2	0.38	0.63	0.07	0.11	0.52	0.66	0.15	0.11	0.25	0.33
3	1.35	0.64	0.50	0.30	1.82	0.67	0.67	0.31	1.97	0.77
4	0.25	0.64	0.08	0.11	0.37	0.67	0.22	0.11	0.18	0.30
5	0.46	1.19	0.46	1.28	0.70	1.26	0.83	1.43	0.72	1.09
6	0.14	0.32	0.10	0.07	0.29	0.35	0.30	0.08	0.09	0.15
7	0.29	0.62	0.62	1.47	0.51	0.67	0.97	1.58	0.42	0.52
8	0.17	0.13	0.16	0.04	0.41	0.15	0.56	0.04	0.08	0.10
9	0.20	0.12	0.20	0.12	0.47	0.14	0.69	0.14	0.17	0.18
THD	1.56	1.78	0.97	1.98	2.22	1.88	1.74	2.16	2.17	1.53

Table A.11: Voltage harmonics 10-min 95%. Compensated values.

Flicker model	EAF Measurement								Random Noise	
Source model	V/Z				I				V/Z	
EAF type	Bucket		Continuous		Bucket		Continuous		N/A	
Software	DPF	PSCAD	DPF	PSCAD	DPF	PSCAD	DPF	PSCAD	DPF	PSCAD
2	0.34	0.50	0.07	0.11	0.51	0.53	0.12	0.11	0.32	0.30
3	0.61	0.94	0.33	0.52	0.94	1.01	0.53	0.55	1.24	1.20
4	0.17	0.28	0.04	0.06	0.28	0.31	0.16	0.07	0.20	0.17
5	0.42	0.74	0.78	1.38	0.69	0.83	1.27	1.52	0.85	0.93
6	0.09	0.18	0.02	0.05	0.21	0.21	0.23	0.06	0.17	0.15
7	0.14	0.30	0.33	0.73	0.30	0.36	0.64	0.85	0.45	0.54
8	0.05	0.11	0.02	0.03	0.24	0.14	0.41	0.04	0.16	0.14
9	0.05	0.13	0.07	0.15	0.27	0.17	0.51	0.18	0.29	0.34
THD	0.85	1.38	0.91	1.66	1.40	1.52	1.68	1.85	1.66	1.69

Table A.12: Voltage harmonics 10-min 95%. Uncompensated values.

A.1.1.8 Voltage Interharmonics at 33 kV

Voltage interharmonics % of rated voltage.

Flicker model	EAF Measurement								Random Noise	
Source model	V/Z				I				V/Z	
EAF type	Bucket		Continuous		Bucket		Continuous		N/A	
Software	DPF	PSCAD	DPF	PSCAD	DPF	PSCAD	DPF	PSCAD	DPF	PSCAD
2	0.58	0.77	0.12	0.15	0.80	0.81	0.27	0.15	0.60	0.52
3	0.59	0.69	0.15	0.13	0.80	0.72	0.29	0.14	0.73	0.57
4	0.28	0.85	0.11	0.19	0.47	0.89	0.37	0.19	0.25	0.42
5	0.25	0.51	0.14	0.17	0.44	0.55	0.39	0.18	0.32	0.42
6	0.19	0.38	0.16	0.11	0.45	0.42	0.48	0.12	0.15	0.24
7	0.22	0.22	0.21	0.9	0.52	0.25	0.61	0.11	0.20	0.25
8	0.26	0.16	0.25	0.05	0.79	0.19	0.99	0.06	0.13	0.16
9	0.29	0.10	0.28	0.04	0.68	0.13	0.86	0.05	0.15	0.17

Table A.13: Voltage interharmonics 10-min 95%. Compensated values.

Flicker model	EAF Measurement								Random Noise	
Source model	V/Z				I				V/Z	
EAF type	Bucket		Continuous		Bucket		Continuous		N/A	
Software	DPF	PSCAD	DPF	PSCAD	DPF	PSCAD	DPF	PSCAD	DPF	PSCAD
2	0.38	0.59	0.08	0.14	0.59	0.63	0.19	0.14	0.48	0.42
3	0.33	0.52	0.09	0.14	0.53	0.57	0.23	0.15	0.70	0.54
4	0.20	0.34	0.06	0.09	0.35	0.39	0.27	0.10	0.39	0.31
5	0.17	0.32	0.06	0.11	0.34	0.37	0.30	0.12	0.53	0.44
6	0.11	0.22	0.03	0.07	0.29	0.26	0.36	0.08	0.32	0.27
7	0.09	0.19	0.04	0.08	0.31	0.24	0.46	0.09	0.42	0.37
8	0.06	0.14	0.02	0.04	0.48	0.22	0.71	0.05	0.27	0.25
9	0.05	0.12	0.02	0.05	0.39	0.20	0.64	0.06	0.34	0.31

Table A.14: Voltage interharmonics 10-min 95%. Uncompensated values.

DEPARTMENT OF SOME SUBJECT OR TECHNOLOGY
CHALMERS UNIVERSITY OF TECHNOLOGY
Gothenburg, Sweden
www.chalmers.se

AVANCEZ
1829

CHALMERS
UNIVERSITY OF TECHNOLOGY